**Atmospheric
Chemistry
and Physics**
Discussions

Open Access

Direct measurements of OH and other product yields from the HO₂ + CH₃C(O)O₂ reaction

F. A. F. Winiberg[1,a], T. J. Dillon[2,3], S. C. Orr[1], C. B. M Groß[2,b], I. Bejan[1,c],
C. A. Brumby[1], M. J. Evans[3,4], S. C. Smith[1], D. E. Heard[1,5], and P. W. Seakins[1,5]

[1]School of Chemistry, University of Leeds, Leeds, LS2 9JT, UK
[2]Max Planck Institute for Chemistry, Division of Atmospheric Chemistry, 55128 Mainz, Germany
[3]Wolfson Atmospheric Chemistry Laboratories, Department of Chemistry, University of York, YO10 5DD, UK
[4]National Centre for Atmospheric Science, University of York, YO10 5DD, UK
[5]National Centre for Atmospheric Science, University of Leeds, Leeds, LS2 9JT, UK
[a]now at: JPL, Pasadena, CA 91106, USA
[b]now at: SCHOTT AG, Physical Analytics, Hattenbergstraße 10, 55122, Mainz, Germany
[c]now at: Faculty of Chemistry and "Integrated Centre for Environmental Science Studies in the North-East Development Region – CERNESIM", University "Al. I. Cuza" of Iasi, Iasi, Romania

Title Page

Abstract	Introduction
Conclusions	References
Tables	Figures

|◄ | ►|
◄ | ►
Back | Close

Full Screen / Esc

Printer-friendly Version

Interactive Discussion

Title Page

Abstract | Introduction

Conclusions | References

Tables | Figures

◄ | ►►

◄ | ►

Back | Close

Full Screen / Esc

Printer-friendly Version

Interactive Discussion

Abstract

The reaction $CH_3C(O)O_2 + HO_2 \rightarrow CH_3C(O)OOH + O_2$ (Reaction R5a), $CH_3C(O)OH + O_3$ (Reaction R5b), $CH_3 + CO_2 + OH + O_2$ (Reaction R5c) was studied in a series of experiments conducted at 1000 mbar and (293±2) K in the HIRAC simulation chamber.

For the first time, products, ($CH_3C(O)OOH$, $CH_3C(O)OH$, O_3 and OH) from all three branching pathways of the reaction have been detected directly and simultaneously. Measurements of radical precursors (CH_3OH, CH_3CHO), HO_2 and some secondary products HCHO and HCOOH further constrained the system. Fitting a comprehensive model to the experimental data, obtained over a range of conditions, determined the branching ratios $\alpha_{(R5a)} = 0.37\pm0.10$, $\alpha_{(R5b)} = 0.12\pm0.04$ and $\alpha_{(R5c)} = 0.51\pm0.12$ (errors at 2σ level). Improved measurement/model agreement was achieved using $k_{(R5)} = (2.4\pm0.4)\times10^{-11}$ cm^3 molecule^{-1} s^{-1}, which is within the large uncertainty of the current IUPAC and JPL recommended rate coefficients for the title reaction. The rate coefficient and branching ratios are in good agreement with a recent study performed by Groß et al. (2014b); taken together, these two studies show that the rate of OH regeneration through Reaction (R5) is more rapid than previously thought. GEOS-Chem has been used to assess the implications of the revised rate coefficients and branching ratios; the modelling shows an enhancement of up to 5 % in OH concentrations in tropical rainforest areas and increases of up to 10 % at altitudes of 6–8 km above the equator, compared to calculations based on the IUPAC recommended rate coefficient and yield. The enhanced rate of acetylperoxy consumption significantly reduces PAN in remote regions (up to 30 %) with commensurate reductions in background NO_x.

1 Introduction

Organic peroxy radicals, RO_2, play a key role in atmospheric chemistry, impacting on the tropospheric HO_x (OH and HO_2) cycle and the O_3 budget. The reaction of OH with volatile organic compounds (VOCs) produces RO_2 radicals which have two main

destruction pathways: (i) reaction with NO and (ii) reaction with HO_2 or other RO_2 radicals. In areas where reaction with NO dominates the RO_2 loss (typically when [NO] > 100 pptv), RO_2 radicals rapidly react with NO forming NO_2 and recycling OH, through the creation and destruction of HO_2 (Reactions R1–R3). By day, the NO_2 produced in these cycles is converted to O_3, a primary component in photochemical smog.

$$RO_2 + NO \rightarrow RO + NO_2 \tag{R1}$$
$$RO + O_2 \rightarrow R'CHO + HO_2 \tag{R2}$$
$$HO_2 + NO \rightarrow OH + NO_2 \tag{R3}$$
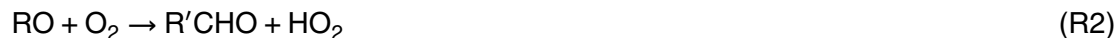
However, in very low NO_x environments (e.g., remote forested areas or over the marine boundary layer) loss of RO_2 is dominated by reaction with HO_2 and other RO_2 radicals (Reactions R4a–R4c); previously considered as important radical termination processes (Lightfoot et al., 1992; Tyndall et al., 2001) with several possible products depending on the structure of the R group. For small alkylperoxy radicals, reaction with HO_2 predominantly produces an organic peroxide (ROOH) through Reaction (R4a). This process is a radical sink in the atmosphere, as a fraction of the water soluble peroxide is lost before radicals are regenerated by photolysis. Observations of ROOH are important as they can be used as an indication of the oxidative capacity of the troposphere (Phillips et al., 2013) and uptake onto aqueous aerosol may influence S(IV) to S(VI) conversion (Lee et al., 2000).

$$RO_2 + HO_2 \rightarrow ROOH + O_2 \tag{R4a}$$
$$\rightarrow ROH + O_3 \tag{R4b}$$
$$\rightarrow OH + RO + O_2 \tag{R4c}$$

More recent research has shown that radical termination may not be the exclusive reaction pathway for certain RO_2 radicals. Hasson et al. (2004) observed, using chamber studies and measuring stable products, that certain peroxy radical +

hydroperoxy radical reactions such as the title reaction of acetylperoxy, $CH_3C(O)O_2$, can lead to the formation of OH radicals through a third channel (Reaction R5c). Previous studies had assumed radical termination through channels R5a ($\alpha_{(R5a)} = k_{(R5a)}/k_{(R5)} = 0.8$) and R5b ($\alpha_{(R5b)} = k_{(R5b)}/k_{(R5)} = 0.2$) (Lightfoot et al., 1992; Moortgat et al., 1989; Crawford et al., 1999). Orlando and Tyndall (2003) were able to demonstrate that an underestimated IR cross-section for peracetic acid, $CH_3C(O)OOH$ (Reaction R5a), had led to the assignment of $\alpha_{(R5a)}$ three times too high. Based on this revised cross-section, Hasson et al. (2004) measured yields of (0.40 ± 0.16) : (0.20 ± 0.08) : (0.40 ± 0.16) for $\alpha_{(R5a)} : \alpha_{(R5b)} : \alpha_{(R5c)}$. In equivalent reactions of the alkyl peroxy radical, $C_2H_5O_2$, with HO_2, only channel (Reaction R4a) producing C_2H_5OOH + O_2 was observed. Clearly the nature of the peroxy radical influences this branching ratio (Orlando and Tyndall, 2012).

$$CH_3C(O)O_2 + HO_2 \rightarrow CH_3C(O)OOH + O_2 \hspace{3cm} \text{(R5a)}$$
$$\rightarrow CH_3C(O)OH + O_3 \hspace{3cm} \text{(R5b)}$$
$$\rightarrow CH_3 + CO_2 + OH + O_2 \hspace{3cm} \text{(R5c)}$$

$CH_3C(O)O_2$ is of particular importance to tropospheric chemistry as it is formed from the oxidation and photolysis of several abundant VOCs. In high NO_x environments, $CH_3C(O)O_2$ leads to the formation of peroxyacetyl nitrate (PAN), a key contributor to long range NO_x transport (Wayne, 1991). It is a significant product of the atmospheric oxidation of isoprene (C_5H_8), the most abundant VOC in certain forests and has been linked to an unexplainably high OH concentrations in field campaigns over low NO_x forested environments (Lelieveld et al., 2008; Whalley et al., 2011; Pugh et al., 2010; Stone et al., 2012; Hofzumahaus et al., 2009; Carslaw et al., 2001; Lou et al., 2010).

A number of mechanisms have also been postulated to explain these higher than expected observed OH concentrations under low NO_x conditions, including the formation and subsequent photolysis of hydroperoxy-aldehyde (HPALD) species (Peeters and Muller, 2010; Peeters et al., 2009; Taraborrelli et al., 2012; Wolfe et al., 2012) and epoxide formation (Paulot et al., 2009). The OH yield from (Reaction R4)

for substituted RO_2 radicals has been put forward as a potential explanation for the shortfall in the [OH] prediction under these conditions (Taraborrelli et al., 2009, 2012; Lelieveld et al., 2008) although at best it merely conserves total HO_x concentrations. Stone et al. (2012) have shown that further amplification of OH in the isoprene mechanism is needed. However, the importance of the kinetics and products of RO_2 + HO_2 chemistry as a radical terminating step under low to moderate NO_x conditions should not be understated. Overall, the kinetics and products of RO_2 + HO_2 is central to the troposphere of the atmosphere especially in the low NO_x environments which are pervasive outside of the industrialized regions of the planet.

A number of studies on the title reaction have taken place with contradictory results as summarised in Jenkin et al. (2007). The results of Jenkin et al. (2007) are in excellent agreement with Hasson et al. (2004) reporting $\alpha_{(R5a)} : \alpha_{(R5b)} : \alpha_{(R5c)}$ of $(0.40 \pm 0.16) : (0.20 \pm 0.08) : (0.40 \pm 0.16)$. These indirect observations of channel (Reaction R5c) have been supported by the direct observation of OH using calibrated laser induced fluorescence (LIF), by Dillon and Crowley (2008). Dillon and Crowley also reported smaller but significant OH yields for the reactions of three other carbonyl-containing RO_2. In their most recent work (Groß et al., 2014b), a Transient Absorption Spectroscopy (TAS) detection system was coupled to a calibrated LIF apparatus to enable a more comprehensive study of Reaction (R5). The reactant radicals HO_2 and RO_2, and the channel (Reaction R5b) product O_3 were monitored by TAS, along with OH (or deuterated OD) by LIF. Experiments were conducted over a range of pressures ($\sim$ 133–667 mbar), with yields of $\alpha_{(R5b)} = 0.16 \pm 0.08$ and $\alpha_{(R5c)} = 0.61 \pm 0.09$ reported, independent of pressure. This is the highest reported OH yield to date, however Groß et al. (2014b) argue that the more comprehensive measurement of reactants and products in an experiment that is not affected by heterogeneous wall losses of organics and radicals (as in the previous chamber based studies), has allowed for a more accurate determination of $\alpha_{(R5c)}$. Groß et al. also reported a higher than recommended (Atkinson et al., 2006) total rate of reaction coefficient for $k_{(R5)} = (2.1 \pm 0.4) \times 10^{-11} \, cm^3 \, molecule^{-1} \, s^{-1}$, independent of pressure. In contrast to the above

work, the combined experimental and theoretical study of Le Crâne et al. (2006) using flash photolysis and monitoring peroxy radicals directly via UV reported no evidence of channel (Reaction R5c) and set an upper limit of 10 % on OH production. Clearly this reaction requires more attention to clarify reaction yields and assess impact on HO_x levels.

Reaction (R5) has been the subject of two theoretical investigations. Firstly, Hasson et al. (2005) calculated the reaction potential energy surface (PES) using CBS-QB3 at the B3LYP/6-311G (2d, d, p) level. The reaction was shown as proceeding either via a triplet surface to $CH_3C(O)OOH + O_2$ (Reaction R5a) or a singlet surface forming a hydrotetroxide intermediate which can decompose to form either $OH + CH_3C(O)O + O_2$ (Reaction R5c) via HO_3 formation or $CH_3C(O)OH + O_3$ (Reaction R5b) through hydrogen exchange. The calculations suggest that channel (Reaction R5c) is considerably less exothermic than the (Reaction R5b) channel (-8.79 and $-113.9\,kJ\,mol^{-1}$ respectively), however, master equation calculations suggested that chemical activation of the initially formed $HO_2 - CH_3C(O)O_2$ adduct combined with a loose transition state, allowed for the observations to be rationalised. Subsequently, Le Crâne et al. (2006) constructed a similar PES using Density Functional Theory (DFT) at the B3LYP/6-31G(d, p) level. The low exothermicity of the (Reaction R5c) channel ($-12.98\,kJ\,mol^{-1}$) compared to the Reaction (R5b) channel ($-82.9\,kJ\,mol^{-1}$) was cited as the dominating factor in the experimentally low OH yields reported (< 0.1). Variations in the thermochemical calculations of the two studies and the interesting enhancement of the OH channel (0.61–0.81) upon deuteration (DO_2) (Groß et al., 2014b) suggest scope for further calculations.

Reported here are the results from the first experiments conducted using free-radical detection (FAGE for OH and HO_2), under simulated ambient conditions. The simultaneous and direct detection of R5 precursors, reactants and products, using FTIR, gas chromatography and an O_3 analyser offered unprecedented, detailed coverage of the key species. This study therefore combined the advantages of the previous chamber studies by Hasson et al. (2004) and Jenkin et al. (2007)

Direct measurements of OH and other product yields from the HO_2 + $CH_3C(O)O_2$ reaction

F. A. F. Winiberg et al.

Title Page

Abstract	Introduction
Conclusions	References
Tables	Figures

|◄ | ►|

◄ | ►

Back | Close

Full Screen / Esc

Printer-friendly Version

Interactive Discussion

and the direct OH detection experiments of Dillon and Crowley (2008) and Groß et al. (2014a, b). The implications of the study have been assessed using a global chemical transport model's (GEOS-Chem) predictions of OH, O_3, NO and PAN concentrations with the revised values of rate coefficient and yields compared to those of the IUPAC recommendation.

2 Experimental

2.1 Chamber and instrumentation

Experiments were performed in the HIRAC (Highly Instrumented Reactor for Atmospheric Chemistry) chamber at 1000 mbar total pressure of a synthetic air mixture ($4 : 1$, $N_2 : O_2$, Zero Grade, BOC) at a constant temperature (293 ± 2 K). HIRAC is a stainless steel chamber with a total volume of $2.25\,m^3$, with multiple access ports used to connect an array of instrumentation and monitoring equipment (pressure gauges, thermocouples, etc.). Further details on the construction can be found in Glowacki et al. (2007a) and Malkin et al. (2010).

Black lamps, housed in eight quartz tubes, were used to initiate photochemistry (Phillips, TL-D 36W/BLB, $\lambda = 350$–400 nm). The lamp housings were flushed with N_2 to regulate the temperature and remove photolabile species (Winiberg et al., 2015). The lamps induced a temperature increase of ~ 2 K in the chamber over the course of a typical experiment (< 40 min). Further information on lamp characterisation is available in the Supplement.

$CH_3C(O)OH$, $CH_3C(O)OOH$, HCHO, and HCOOH, along with chemical precursors CH_3CHO, and CH_3OH, were detected using FTIR. The multipass modified Chernin cell was optimised for 72 internal reflections giving an approximate path length of 128.5 m (Glowacki et al., 2007b). Sample IR spectra were recorded as the average of 100 scans (~ 70 s integration period) at $0.5\,cm^{-1}$ resolution. Reference spectra were taken of the compounds in the HIRAC chamber. Analysis of sample FTIR spectra was conducted

at $\sim 2000\,\text{cm}^{-1}$ for CH_3OH and $1600–1800\,\text{cm}^{-1}$ for all other detectable species. Quantitative analysis was aided by a custom written iterative non-linear least squares fitting algorithm (Winiberg, 2014). Supporting online measurements of CH_3OH and CH_3CHO were conducted using gas chromatography with flame ionisation detection (GC-FID), using an evacuated sampling loop into which gas from the chamber was expanded. The GC was fitted with a DB-WAX column (15 m, 0.32 mm, 0.25 μm) using He carrier gas and a constant oven temperature (35 °C) and was able to provide hydrocarbon measurements on a 2 min time resolution. GC measurements were only completed during selected experiments, indicated in the results section.

Ozone concentrations were measured using a UV photometric O_3 analyser (TEC Model 49C, limit of detection (LOD) = 1.0 ppb at 60 s averaging). A trace level chemiluminescence NO_x analyser (TEC Model 42C, LOD = 50 pptv at 60 s averaging) was used to confirm that NO_x concentrations were below the detection level of the apparatus during experiments.

The low pressure LIF based FAGE instrument (Fluorescence Assay by Gas Expansion) was used to detect OH and HO_2 radicals for these experiments. The instrument was used as described previously in the literature (Glowacki et al., 2007a; Malkin et al., 2010; Winiberg et al., 2015). LIF with excitation at 308 nm ($A^2\Sigma^+(v' = 0) \leftarrow X^2\Pi_i(v'' = 0)$ transition) was used to probe the OH radicals directly, and the resulting fluorescence was collected via a (305 ± 5 nm) nm interference filter. Under typical operating conditions, air was sampled at ~ 6 slm through a 1.0 mm diameter pinhole nozzle and passed down the inlet (length 280, 50 mm diameter) into the OH detection axis maintained at low pressure (~ 3.9 mbar) using a high capacity rotary pump-backed roots blower pumping system (Leybold, trivac D40B and ruvac WAU251). The long inlet was used to sample away from the chamber walls where, very close to the wall (< 10 mm), radical losses have been shown to become significant ($\sim 20\%$) (Winiberg et al., 2015).

Concentrations of HO_2 were measured simultaneously in a second detection axis $\sim$ 300 mm downstream of the OH detection axis. High purity NO (BOC, N2.5 Nitric Oxide)

was added ~ 20 mm before the HO_2 detection axis into the centre of the FAGE cell in the direction of gas flow through $1/8''$ stainless steel tubing at a rate of 5 sccm (Brooks 5850S) converting a fraction of HO_2 to OH. The conversion of certain RO_2 radicals (particularly those that yield β-hydroxyperoxy radicals, such as derived from an alkene, or for longer chain aliphatic RO_2) to OH upon reaction with NO in FAGE detections cells (Whalley et al., 2013; Fuchs et al., 2011) have recently been shown to give a significant enhancement of the HO_2 signal. These effects have been thoroughly studied using a range of different hydrocarbons for the HIRAC FAGE apparatus and will be the subject of a further publication. The reaction scheme used to model the $CH_3C(O)O_2 + HO_2$ system did not generate any β-hydroxyperoxy radicals, hence negligible interference was assumed under the conditions of these experiments.

Laser light was generated using a pulsed Nd:YAG (JDSU Q201-HD) pumped dye laser (SIRAH Cobra) operating at 5 kHz pulse repetition frequency. The laser power entering each fluorescence cell was typically 7–10 and 3–5 mW for the OH and HO_2 cells, respectively. The FAGE instrument was calibrated using the H_2O vapour photolysis method detailed in Winiberg et al. (2015), and was shown to have a typical uncertainty of 38 % (2σ) and a limit of detection of 1.6×10^6 molecule cm^{-3} at 60 s averaging and for a signal-to-noise ratio of unity.

2.2 Chemicals, sample preparation and gas handling

Liquid samples of CH_3OH (> 99.93 %, Sigma Aldrich), HCOOH (> 98 %, Sigma Aldrich), $CH_3C(O)OH$ (> 99 %, Sigma Aldrich), $CH_3C(O)OOH$ (40 % in acetic acid, Sigma Aldrich) were injected into the synthetic air filled HIRAC chamber directly using 100 (± 5) and 10 (± 0.5) µL syringes. Gas samples of CH_3CHO (> 99.5 %, Sigma Aldrich), Cl_2 (99.9 %, Gas Products Ltd.) and HCHO were expanded into the stainless steel delivery vessel before being flushed into HIRAC using high purity N_2. Formaldehyde was prepared for gas delivery upon heating para-formaldehyde (99 %, Sigma Aldrich). Where appropriate, species were purified through several freeze-pump-thaw cycles using liquid nitrogen before injection. Reactants were introduced into

Title Page

Abstract	Introduction
Conclusions	References
Tables	Figures

|◄ | ►|

◄ | ►

Back | Close

Full Screen / Esc

Printer-friendly Version

Interactive Discussion

CC BY

the chamber individually, allowing ~ 90 s mixing time before stability was confirmed by 5–10 FTIR measurement spectra and the photolysis lamps were turned on.

2.3 Radical generation and experimental process

Table 1 contains the starting conditions for 12 individual experiments (labelled as P1–P12) conducted at 1000 mbar and 293 K. Acetylperoxy and HO_2 radicals were generated through the chlorine atom initiated oxidation of CH_3CHO and CH_3OH respectively:

$$Cl_2 + h\nu \rightarrow 2Cl \tag{R6}$$
$$Cl + CH_3OH \rightarrow CH_2OH + HCl \tag{R7}$$
$$CH_2OH + O_2 \rightarrow HCHO + HO_2 \tag{R8}$$
$$Cl + CH_3CHO \rightarrow CH_3CO + HCl \tag{R9}$$
$$CH_3CO + O_2(+M) \rightarrow CH_3C(O)O_2(+M) \tag{R10}$$

The rate coefficients for the Cl atom reactions are well established (Seakins et al., 2004; Atkinson et al., 2008) and hence by varying the initial ratio $[CH_3OH]_0 : [CH_3CHO]_0$ it was possible to control the initial radical ratio $[HO_2] : [CH_3C(O)O_2]$ (detailed in Sect. 3.3.1). The CH_3OH was kept in excess (~ 4 : 1) to produce HO_2 in excess, whilst preserving the lifetime of the CH_3CHO. Experiments were conducted over a ~ 600 s time period to ensure that measurements were taken during the initial stages of the reaction where $\Delta[CH_3CHO] < 50\%$. During this time, Cl atom concentrations were controlled by CH_3OH and CH_3CHO rather than reacting with products. Initial Cl atom concentrations are also displayed in Table 1.

Control experiments were conducted to characterise losses of products and reactants to the walls of the chamber and by photolysis. Samples were injected into the chamber at concentrations up to ~ 5×10^{13} molecule cm^{-3} (~ 2 ppm) in synthetic air and were monitored continuously by FTIR and FAGE through several lamps-on, lamps-off photolysis cycles with 2, 4 and 8 lamps (~ 1 h for each stage).

Appreciable wall loss was observed for the organic acids ($\sim 10^{-4}\,\mathrm{s}^{-1}$) and these were characterised and incorporated into the chemical model reaction scheme used (Sect. 2.4). Negligible decay due to photolysis was seen for any species. Trace levels of HO_2 ($\sim 10^8\,\mathrm{molecule\,cm}^{-3}$) were observed upon illumination of HCHO with all 8 lamps, suggesting some photolysis. However, a negligible decay was observed when monitoring HCHO using FTIR over a 60 min photolysis period (standard experiment time ~ 10 min).

2.4 Chemical model

Numerical simulation of the chemical system was necessary to gain quantitative information about $\alpha_{(R5a)}$: $\alpha_{(R5b)}$: $\alpha_{(R5c)}$. Chemical simulations were conducted using the Kintecus numerical integrator package (Ianni, 2002). The comprehensive model mechanism, displayed in Table 2, was constructed from reactions defined in the chamber studies by Hasson et al. (2004) and Jenkin et al. (2007), with updated rate constants where available from IUPAC and JPL (Atkinson et al., 2006; Sander et al., 2011). Simulated rate coefficients $k_{(R5a)}$: $k_{(R5b)}$: $k_{(R5c)}$ were optimised automatically using Kintecus, fitted to the experimentally measured products from Reaction (R5). Experimental data were also compared to simulated traces based on the IUPAC recommendation, $k_{(R5)} = (1.4^{+1.4}_{-0.7}) \times 10^{-11}\,\mathrm{cm}^3\,\mathrm{molecule}^{-1}\,\mathrm{s}^{-1}$ and $\alpha_{(R5a)}$: $\alpha_{(R5b)}$: $\alpha_{(R5c)} = 0.41 : 0.15 : 0.44$ (Atkinson et al., 2006) and the more recent work by Groß et al. (2014b), $k_{(R5)} = (2.1 \pm 0.4) \times 10^{-11}\,\mathrm{cm}^3\,\mathrm{molecule}^{-1}\,\mathrm{s}^{-1}$.

Presented here are two sets of experiments conducted a year apart. There was a decrease in $j(\mathrm{Cl}_2)$ between experiments due to degradation of the lamp with extensive use. Hence, $j(\mathrm{Cl}_2)$ has been determined for each set of experimental data using the measured Cl atom induced decay of the CH_3CHO and CH_3OH reactants. Supporting $j(\mathrm{NO}_2)$ measurements were conducted for all 8 of the black lamps switched on during the later time period, which gave $j(\mathrm{NO}_2) = (2.4 \pm 0.8) \times 10^{-3}\,\mathrm{s}^{-1}$. Using IUPAC recommended absorption cross sections for both NO_2 (Atkinson et al.,

correlating well with the observed reactant decays. The black lamp intensity profiles as
a function of time were entered into Kintecus as a constraint for the photolysis rate (as
described in Sect. 2.1), allowing accurate modelling of the precursor photolysis. Both
5 the predicted [OH] and [HO$_2$] were observed to better correlate with the measured
radical concentrations when using this constraint, compared to starting the model with
a constant photolysis rate.

3   Results and discussion

Figure 1 displays typical reactant decay profiles for CH$_3$CHO and CH$_3$OH
10 for experiment P11, measured simultaneously using FTIR and GC-FID. The
concentrations were determined independently and are in excellent agreement. Similar
agreement was observed for experiments P9 and P10 with an overall correlation of
[GC] : [FTIR] = (0.97 ± 0.03) and (1.05 ± 0.09) for CH$_3$CHO and CH$_3$OH, respectively
(uncertainties representative of the standard deviation in repeated measurement to
15 ±2σ).
Figure 2a, b and c show the product profiles of CH$_3$C(O)OOH, CH$_3$C(O)OH and
O$_3$ respectively as a function of decay in CH$_3$CHO (Δ[CH$_3$CHO]) for experiments P1–
P5, P11 and P12, while Fig. 3 shows OH and HO$_2$ time profiles for experiment P1,
typical of other profiles (see Supplement). For a decrease in [CH$_3$CHO] of $\sim 50\,\%$,
20 near linear increases in [CH$_3$C(O)OOH], [CH$_3$C(O)OH] and [O$_3$] were observed,
suggesting that the rate of formation of stable products through Reaction (R5) remained
constant throughout the $\sim 600\,\text{s}$ reaction period. The monitored prompt increase in
[OH] suggested a primary production channel, maintaining a steady state level of $\sim$
10^7 molecule cm^{-3} throughout the experiment. Concentrations of [HO$_2$] were observed
25 to quickly reach a steady state of $\sim 10^{11}$ molecule cm^{-3} during each experimental run,
providing sufficient HO$_2$ for reaction with CH$_3$C(O)O$_2$. No HO$_2$ data from experiments
P4–P6, P10 and P11 were available due to an error with the mass flow controller

that meters the flow of NO into the FAGE HO_2 detection cell. Both HCHO and HCOOH were detected in experiments P1–P5, P11 and P12 also and are shown as a function of decay in CH_3OH, $\Delta[CH_3OH]$, in Fig. 4a and b respectively. The near-linear increase in [HCHO] supported HO_2 measurements, suggesting that the oxidation of methanol was a constant source of high $[HO_2]$ in the system. HCOOH was observed to increase in concentration at later times, suggesting a secondary source. Supporting measurements of HCOOH were key in evaluating secondary sources of OH, propagated through the reaction of HO_2 with HCHO and described in more detail in Sect. 3.2.

The chemical reaction scheme, detailed in Table 2, was applied to all datasets, fixing the $j(Cl_2)$ and reactant concentrations as shown in Table 1. The values of $k_{(R5)}$ and the branching ratios $\alpha_{(R5a)} : \alpha_{(R5b)} : \alpha_{(R5c)}$, displayed in Table 3, were assigned by fitting the model to the experimental data. The losses of the precursors were predominately controlled by reaction with Cl atoms and Fig. 1 shows the simulated decays of CH_3OH and CH_3CHO which were found to be in excellent agreement with the measured data across all experiments. Due to the crowded nature of the datasets presented in Figs. 2 and 4, only the simulations for experiments P1 and P3 are shown as examples. The prompt increase in measured [OH] suggested production from Reaction (R5), and this was supported by the chemical simulation which shows > 75 % of total [OH] production through channel (Reaction R5c) over the 600 s reaction period (Fig. 3).

When using complex chemical models to determine branching ratios of a target reaction, it is important to demonstrate that the observations are sensitive to the target reaction. The rate of production and destruction analyses shown for OH and HO_2 (Fig. 3) demonstrate that the title reaction dominates OH production and that the rate of OH destruction is determined by only a few, well-characterised reactions, thus OH measurements will be a sensitive test of the branching ratio of Reaction (R5). For HO_2, production and destruction is controlled by a slightly wider number of reactions, however, these too are well-characterised and hence the good agreement between measurement and model for HO_2 suggests that the system is well-determined.

Title Page

Abstract	Introduction
Conclusions	References
Tables	Figures

|◄ | ►|

◄ | ►

Back | Close

Full Screen / Esc

Printer-friendly Version

Interactive Discussion

3.1 Assignment of $k_{(R5)}$ and $\alpha_{(R5a)} : \alpha_{(R5b)} : \alpha_{(R5c)}$

Table 3 contains assigned yields for all experiments conducted at 1000 mbar and 293 K. Uncertainty in the branching ratios determined here were calculated as a function of the precision error in repeated determinations combined with uncertainties in the FTIR, O_3 analyser and FAGE calibrations and is displayed to $\pm 2\sigma$. Yields from the three branching pathways of $CH_3C(O)O_2 + HO_2$ were assigned through application and optimisation of the chemical model to each experimental dataset (Sect. 2.4), detailed in Table 3. Displayed in Fig. 5 are the time dependent concentration profiles for $CH_3C(O)OOH$, $CH_3C(O)OH$, O_3 and OH for experiment P2, representative of a typical experiment. The results are presented against three modelling scenarios each using the same chemistry but with $k_{(R5)}$ and $\alpha_{(R5a)}$: $\alpha_{(R5b)}$: $\alpha_{(R5c)}$ based on: Model1 the IUPAC values (1.4×10^{-11} cm^3 molecule^{-1} s^{-1}, 0.41 : 0.15 : 0.44), Model2 the Gros et al. (2014b) values and Model3 values from the best fit to the current experimental data. Model1 matched the data well for channels (Reactions R5a and b) using $\alpha_{(R5a)} = 0.41$, $\alpha_{(R5b)} = 0.15$. However, in general for all datasets except P1, OH was consistently under predicted by the model with $\alpha_{(R5c)} = 0.44$, with modelled [OH] falling outside of the uncertainty of the FAGE measurements ($\pm 38\%$, 2σ). Clearly the rate of production of OH in our system was underestimated.

Using Model2 in our chemical simulation, the [OH] and [O_3] and [$CH_3C(O)OH$] were reproduced by the model within the uncertainty of the measurements, however the [$CH_3C(O)OOH$] was systematically under predicted (see Fig. 5). Adjusting the parameters $\alpha_{(R5a)} : \alpha_{(R5b)} : \alpha_{(R5c)}$, reasonable agreement between measured and modelled data was observed, well within the uncertainty of the measurements and average yields were determined as (0.38 ± 0.08) : (0.12 ± 0.02) : (0.50 ± 0.08). However, improvement in the measured to modelled agreement for [$CH_3C(O)OOH$] was typically at the expense of predicted [OH]. Therefore the yields shown here are representative of the best fit to both $CH_3C(O)OOH$ and OH that was possible, weighting the assignment to the larger uncertainty in the [OH] determination.

F. A. F. Winiberg et al.

Title Page

Abstract | Introduction

Conclusions | References

Tables | Figures

|◀ | ▶|

◀ | ▶

Back | Close

Full Screen / Esc

Printer-friendly Version

Interactive Discussion

Improved correlation between measured and modelled OH was achieved by fitting k_5 and $\alpha_{(R5a)} : \alpha_{(R5b)} : \alpha_{(R5c)}$ to the measured data from all three branching pathways from the CH$_3$C(O)O$_2$ + HO$_2$ reaction. A non-linear least squares iterative fitting routine built into the Kintecus package was used to determine the best fit rate coefficients by judging the reduced χ^2 (determined using the Powell method; Press et al., 1992; Ianni, 2002). An increase in the rate coefficients for all channels of Reaction (R5) was observed, whilst the ratio of $k_{(R5a)}$ and $k_{(R5b)}$ ($k_{(R5a)}/k_{(R5b)} = 3.2 \pm 0.2$) remained within uncertainty of the IUPAC recommendation (2.73 ± 0.48), leading to an overall increase in $k_{(R5)} = (2.4 \pm 0.4) \times 10^{-11}$ cm^3 molecule^{-1} s^{-1} and average branching ratios of $\alpha_{(R5a)} = 0.37 \pm 0.10$, $\alpha_{(R5b)} = 0.12 \pm 0.04$ and $\alpha_{(R5c)} = 0.51 \pm 0.12$. Uncertainties were taken as the quoted standard errors in the fitting routine to $\pm 2\sigma$. Figure 5 displays the improvement in correlation to the measured data using predicted OH yields from the fitted rate constants.

The OH steady state (SS) concentration ([OH]$_{ss}$) in the chemical system was controlled by the production of OH primarily through Reaction (R5) ($> 60\%$ for entirety of the ~ 600 s reaction time, Fig. 3) whilst OH loss was controlled by its well characterised reactions with CH$_3$CHO and CH$_3$OH at the beginning of the experiment, with HCHO playing an increased role as the experiment progresses (Fig. 3). Reaction of OH with CH$_3$OH is 10^2 slower than the analogous reaction with Cl atoms, and so the predicted [CH$_3$OH] was insensitive to any change in $k_{(R5c)}$. However, the rate coefficient for OH + CH$_3$CHO was only a factor of ~ 5 slower compared to Cl + CH$_3$CHO, and so with the [OH]$_{ss}$ higher than [Cl]$_{ss}$ by a factor of ~ 3, loss of CH$_3$CHO through reaction with OH starts to become competitive (2 : 1 ratio Cl : OH loss) and so a small sensitivity in [CH$_3$CHO] to k_{R5c} was observed.

The increase in $k_{(R5)}$, and therefore rate of loss of CH$_3$CHO, led to an overall reduction in the [CH$_3$C(O)O$_2$]$_{ss}$. The [CH$_3$C(O)O$_2$]$_{ss}$ was controlled primarily through reaction with HO$_2$ and less so through self-reaction and reaction with CH$_3$O$_2$ (Reaction R20) in a $\sim 2 : 1 : 1$ ratio (for this system). The [HO$_2$]$_{ss}$ remained unaffected by an

increase in $[OH]_{ss}$ (minimal change in CH_3OH loss), and the co-product of channel (Reaction R5c) is CH_3O_2 (via Reaction R19), hence the decrease in $[CH_3C(O)O_2]_{ss}$.

Clearly the $[CH_3O_2]_{ss}$ played an important role in the determination of Reaction (R5) yields and was defined by primary production in channel (Reaction R5c), and loss through reaction with $CH_3C(O)O_2$ (Reaction R20), HO_2 and itself. The removal of CH_3O_2 via another reaction could also lead to a discrepancy in yield assignment. Recently, Bossolasco et al. (2014) determined the rate coefficient for the rapid reaction of CH_3O_2 with OH radicals ($k = (2.8 \pm 1.4) \times 10^{-10}$ cm^3 molecule^{-1} s^{-1}). This reaction has been hypothesised to yield a Criegee intermediate as a possible product, and could contribute to significant HCOOH yields in the troposphere in certain environments (Fittschen et al., 2014). Despite the large rate coefficient, this reaction was found to have a negligible effect on the chemical system described here due to the higher concentrations of RO_2 radicals in the system ($\sim 10^{11}$ molecule cm^{-3}), preferentially reacting with CH_3O_2. Assuming that every OH + CH_3O_2 reaction leads to HCOOH (used only as an example), only a small effect was observed on the HCOOH yield ($\sim 2\,\%$), well within the uncertainty in the measurement and model simulation.

Assignment of the yield for channel (Reaction R5c) was found to be insensitive to the ratio of $\alpha_{(R5a)} : \alpha_{(R5b)}$. The ratio of $\alpha_{(R5a)} : \alpha_{(R5c)}$ was observed to affect the $CH_3C(O)OH$ yield, but not that of O_3, suggesting $\alpha_{(R5b)}$ was also unaffected. Reaction (R5b) was found to be the dominant production channel for $CH_3C(O)OH$ ($\sim 80\,\%$) with a $\sim 19\,\%$ yield from the reaction of $CH_3C(O)O_2$ with CH_3O_2 (Reaction R20b). As the dominant production channel for CH_3O_2 in the system was the decomposition of acetylalkoxy radicals (Reaction R19) produced alongside OH in (Reaction R5c) also produced here from Reaction (R20a), a certain sensitivity for $CH_3C(O)OH$ to $\alpha_{(R5c)}$ can be expected. Modelled profiles for both O_3 and $CH_3C(O)OH$ were in good agreement with measurements from two independent techniques, improving confidence in the determination of $\alpha_{(R5b)}$ and suggesting that secondary chemistry was well characterised in the reaction scheme. Predicted concentrations of HCHO and

HCOOH were found to be insensitive to the increased rate constant as their dominant removal was through reaction with Cl radicals ($\sim 10^2$ faster than reaction with OH).

3.2 Secondary OH production

The sum of OH sources from secondary $RO_2 + HO_2$ reactions (Fig. 3) showed negligible impact on the measured [OH] until $\sim 200\,s$, and in total were still the minor production channels even at $t = 600\,s$ ($\sim 30\%$). Secondary OH was primarily produced through the reaction of Cl with CH_3OOH and $HOCH_2O_2$ with HO_2 (Reaction R12), the RO_2 radical produced from the association of HO_2 and HCHO (Reaction R11). Reaction (R12) is thought to proceed through three possible channels, producing a hydroxyl-alkoxy radical, $HOCH_2O$ (Reaction R12a), a hydroxyperoxide, $HOCH_2OOH$ (Reaction R12b) and HCOOH (Reaction R12c) in a $0.5 : 0.3 : 0.2$ ratio (Jenkin et al., 2007).

$$HCHO + HO_2 \leftrightarrow HOCH_2O_2 \qquad\qquad (R11, R-11)$$

$$HOCH_2O_2 + HO_2 \rightarrow HOCH_2O + OH + O_2 \qquad\qquad (R12a)$$
$$\rightarrow HOCH_2OOH + O_2 \qquad\qquad (R12b)$$
$$\rightarrow HCOOH + H_2O + O_2 \qquad\qquad (R12c)$$

While Reaction (R11) has received minor attention in the literature (Veyret et al., 1989; Barnes et al., 1985; Rohrer and Berresheim, 2006), to date the subsequent RO_2 reactions with HO_2 have only been studied by Jenkin et al. (2007). During their investigation of the title reaction, photolysis of Cl_2 was used with a CH_3OH/benzene mixture with the aim of detecting any OH produced from Reaction (R12a), using benzene as a chemical tracer for OH. Jenkin et al. (2007) deduced that the chemical model better reproduced the experimentally measured HCHO, HCOOH and OH upon inclusion of the $HOCH_2O_2$ self-reaction (Reaction R13), the assumed instantaneous

F. A. F. Winiberg et al.

Title Page

Abstract | Introduction

Conclusions | References

Tables | Figures

|◄ | ►|

◄ | ►

Back | Close

Full Screen / Esc

Printer-friendly Version

Interactive Discussion

reaction of HOCH$_2$O with O$_2$ (Reaction R14), and the Cl initiated oxidation of HOCH$_2$OOH (Reactions (R15) and (R16). At the experimental temperatures, the rates of Reactions (R11) and (R-11) are close to being in equilibrium with only a small amount of HOCH$_2$O$_2$ reacting via other pathways (shown as HO$_2$ + HCHO net loss in HO$_2$ RODA (rate of destruction analysis) in Fig. 3).

$$HOCH_2O_2 + HOCH_2O_2 \rightarrow HOCH_2O + HOCH_2O + O_2 \qquad \text{(R13a)}$$
$$\rightarrow HCOOH + HOCH_2OH + O_2 \qquad \text{(R13b)}$$

$$HOCH_2O + O_2 \rightarrow HCOOH + HO_2 \qquad \text{(R13)}$$
$$Cl + HOCH_2OOH \rightarrow HOCHOOH + HCl \qquad \text{(R14)}$$
$$HOCHOOH \rightarrow HCOOH + OH \qquad \text{(R15)}$$

As such, these reactions and their respective rate constants determined by Jenkin et al. (2007) have been included in the chemical model presented here (Table 2). The good agreement between experimental and simulated HCHO and HCOOH (Fig. 4) and the OH at longer times (Fig. 3) show that we are in agreement with the evaluation of OH yields presented by Jenkin et al. (2007). It should be noted, however, that HCOOH showed the largest discrepancy between measured and modelled data overall.

The sensitivity of the uncertainty in the analogous HO$_2$ association with CH$_3$CHO (Reaction R17) on the measured products was also investigated. To date, only one study exists into the equilibrium (Tomas et al., 2001), therefore uncertainty in the equilibrium constant could impact on OH and CH$_3$C(O)OH yields through further reactions of the CH$_3$CH(OH)O$_2$ radical with HOCH$_2$O$_2$ and CH$_3$O$_2$ (see Table 2).

$$CH_3CHO + HO_2 \leftrightarrow CH_3CH(OH)O_2 \qquad \text{(R16)}$$
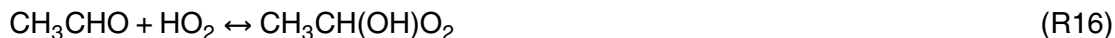
The chemical model showed that the dominating pathway for removal of CH$_3$CHO was through reaction with HO$_2$ at $\sim 90\%$. However, the rate of dissociation from CH$_3$C(OH)O$_2$ back to CH$_3$CHO and HO$_2$ was $> 99\%$ of the total CH$_3$C(OH)O$_2$ loss.

Hence, negligible $[CH_3C(OH)O_2]_{ss}$ was formed and the further reaction with other RO_2 species or HO_2 was negligible. Finally, the model was found to be insensitive to the removal of this pathway from the mechanism entirely.

3.3 Sensitivity of the chemical system to initial conditions

3.3.1 Precursor ratio, $[CH_3OH]_0 : [CH_3CHO]_0$

By manipulating the starting ratio of $[CH_3OH]_0 : [CH_3CHO]_0$ it was possible to control the ratio of $HO_2 : CH_3C(O)O_2$ during a given experiment and $[CH_3OH]_0 : [CH_3CHO]_0$ ratios between 0.0–5.6 were studied. The observed $CH_3C(O)OOH$, $CH_3C(O)OH$ and O_3 experimentally determined product yields were calculated as the gradient from the linear regression of a plot of respective Δ [product] vs. $\Delta[CH_3CHO]$. O_3 data were unavailable for experiments P6 and P7 due to a software error. The yields are graphically displayed as a function of $[CH_3OH]_0 : [CH_3CHO]_0$ in Fig. 6. The product yields were observed to remain at a maximum between ratios of 1.2 and 5.6, with yields decreasing towards experiments where no methanol was added (ratio = 0.0). This indicated that for experiments conducted at $[CH_3CHO]_0 : [CH_3OH]_0 \approx 4$, product yields from Reaction (R5) were still maximised, but interference was minimized from the saturated CH_3OH v_1 stretch absorption on the surrounding spectrum ($\sim 1000\,cm^{-1}$).

Each experiment was simulated using Model3. Compared to experiments using a CH_3OH precursor, the chemistry in experiments P8 and P9 was driven by the Cl atom initiated oxidation of CH_3CHO. Hence RO_2 chemistry outside of reaction with HO_2 drives product formation. The initial dominating loss for $CH_3C(O)O_2$ is self-reaction (Reaction R18), followed closely by reaction with CH_3O_2 (Reaction R20), produced through Reaction (R19). The required HO_2 radicals were produced at later times from the Cl initiated oxidation of HCHO (Reaction R21), itself produced from reaction for CH_3O_2 with $CH_3C(O)O_2$ (Reaction R20b). As the HCHO is produced quickly through the abundant $[RO_2]$, no significant delay in Reaction (R5) product formation was observed on the timescale of the measurements presented here, however the reduced

yields were calculated as there was no excess of HO_2 in the system. This trend has been reported and reproduced in the literature (Jenkin et al., 2007; Hasson et al., 2004).

$$2CH_3C(O)O_2 \rightarrow 2CH_3C(O)O + O_2 \qquad \text{(R17)}$$

$$CH_3C(O)O + O_2 \rightarrow CH_3O_2 + CO_2 \qquad \text{(R18)}$$

$$CH_3C(O)O_2 + CH_3O_2 \rightarrow CH_3C(O)O + CH_3O + O_2 \qquad \text{(R20a)}$$
$$\rightarrow CH_3C(O)OH + HCHO + O_2 \qquad \text{(R20b)}$$

$$Cl + HCHO + O_2 \rightarrow CO + HO_2 + HCl \qquad \text{(R20)}$$
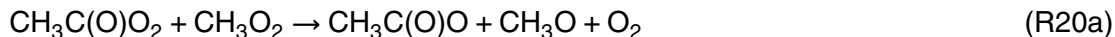
Displayed in Fig. 7 are the measured and modelled product yields of OH and HO_2, (Fig. 7a), $CH_3C(O)OOH$ and $CH_3C(O)OH$, (Fig. 7b), O_3, (Fig. 7c) and HCHO, (Fig. 7d), as a function of time for experiment P9 where $[CH_3OH]_0 = 0$. The simulation was completed using $k_{(R5)} = (2.4 \pm 0.4) \times 10^{-11}\,\text{cm}^3\,\text{molecule}^{-1}\,\text{s}^{-1}$ and the branching ratios were optimised to fit the data ($\alpha_{(R5a)} = 0.42 \pm 0.05$, $\alpha_{(R5b)} = 0.14 \pm 0.04$ and $\alpha_{(R5c)} = 0.44 \pm 0.10$) of that experiment. Excellent agreement between the measured and modelled decay of CH_3CHO was observed, which was additionally constrained by measurements from the GC-FID and FTIR, and good agreement between the measured and modelled OH, HO_2, $CH_3C(O)OOH$ and HCHO was also seen (Fig. 7, Model3 data). The model predicted a rapid increase in [OH] at time $> 400\,\text{s}$, however in experiment P9, the measured OH appears to remain constant. The simulation suggests that after $> 400\,\text{s}$, the OH yield from Reactions (R12a) and (R15)–(R16) start to dominate as the CH_3CHO in the system is depleted, however as no OH and HO_2 data were recorded past $\sim 450\,\text{s}$ for both experiments P8 and P9, we are unable to comment if the discrepancy from the model 8 increased at later times.

The simulation over predicted $[CH_3C(O)OH]$ by a factor of ~ 2 towards the end of the reaction period ($\sim 600\,\text{s}$) for both experiments P8 and P9. The two main production channels for $CH_3C(O)OH$ are through Reactions (R5b) and (R20b), and in experiment

P9 the chemical model 12 predicted the flux through both channels was in competition for the first $\sim 200\,\mathrm{s}$ of the Reaction (R20b) > (Reaction R5b) by $\sim 25\,\%$. Modifying the branching ratio for Reaction (R20b) in the chemical simulation from 0.1 to 0.03 showed better agreement with measured data in experiment P9 (Fig. 7, Model3a) and kept the branching ratio well within the IUPAC recommended uncertainty of 16 ± 0.1. Models conducted for $[CH3OH]0 : [CH3CHO]0 > 1.0$ were found to be insensitive to a change in the $k_{(R20)}$ branching ratio.

An over-prediction of CH_3O_2 in the chemical model could also increase $CH_3C(O)OH$ through Reaction (R20). However, measurement of HCHO in experiment P9 (Fig. 7d) was well matched by the modelled profile (Fig. 7d, Model3a), calculated through the primary production, Reactions (R20a) and (R23) and self-reaction of CH_3O_2 (Reactions R22 and R23), suggesting the CH_3O chemistry in the system was well understood under these conditions.

$$2CH_3O_2 \rightarrow 2CH_3O + O_2 \tag{R22a}$$
$$\rightarrow CH_3OH + HCHO + O_2 \tag{R22b}$$

$$CH_3O + O_2 \rightarrow HCHO + HO_2 \tag{R22}$$

These experiments conducted at $[CH_3OH]_0 = 0$ have showed that the CH_3CHO and surrounding peroxy chemistry was well characterised by the comprehensive model in Table 2.

3.3.2 Photolysis rate, $j(Cl_2)$

The target reaction was studied using 2, 4 and 8 photolysis lamps at 1000 mbar and 293 K, preserving $[CH_3OH]_0 : [CH_3CHO]_0 \approx 4$. Photolysis rates for all experiments are displayed in Table 1. Photolysis rates differed between experiments P1–P5 and P6–P12 with the same number of lamps due to the degradation of the lamp emission intensity over time (see Sect. 2). The initial $[Cl_2]_0$ was lowered in experiments P4, P5

and P12 in an attempt to maintain the Cl atom and therefore overall radical density inside the chamber ($[Cl]_0 \approx 5 \times 10^6$ molecule cm^{-3}), compared to experiments P1–P3 and P11. The stable product yields ($CH_3C(O)OOH$, $CH_3C(O)OH$, O_3, HCHO and HCOOH) from experiments P4, P5 and P12 were found to be in excellent agreement with the experiments conducted at a lower photolysis rate and are displayed in alongside each other in Figs. 2 and. 4. When $k_{(R5)}$ and $\alpha_{(R5a)} : \alpha_{(R5b)} : \alpha_{(R5c)}$ were determined using the chemical simulation, good agreement was observed between the higher photolysis rate experiments and those conducted with only two lamps, confirming minimal product loss via photolysis and a good control over the experimental conditions in the chamber.

3.3.3 Interferences and uncertainties

Accurate determination of product yields in chamber experiments where chemical systems are complex is a non-trivial task. Interferences and measurement uncertainties need to be carefully considered to accurately quote rate constants and branching ratios. In this study possible systematic errors from IR measurements (deconvolution and IR cross-sections), O_3 and OH interferences were considered and a detailed analysis is presented in the Supplement.

The excellent agreement between GC and FTIR measurements suggests that concentrations extracted from FTIR measurements are correct. The high concentrations of aromatics that have been shown to cause interferences in O_3 absorption instruments (Kleindienst et al., 1993) are absent in these studies and the good agreement between $CH_3C(O)OH$ and O_3 (the two products of channel R5b) again suggests no significant interference.

Recent studies have highlighted interferences in some FAGE based OH measurements (Mao et al., 2012; Novelli et al., 2014), typically involving sampling from systems containing high concentrations of O_3 and alkenes, with evidence presented consistent with the interference being due to the decomposition of stabilised Criegee intermediates. A number of possible scenarios could give rise to interferences, but

a detailed analysis of the conditions plus appropriate experimental background checks, as detailed in the Supplement, suggests that there negligible interferences to our OH measurements.

3.4 Comparison with literature data

The average branching ratios determined for Reaction (R5) at 1000 mbar and 293 K using the recently reported value for $k_{(R5)}$ from Groß et al. (2014b) as well as those determined using the fitting of the chemical model are presented in Table 4, together with previous reported values. Previous measurements of $k_{(R5)}$ by Moortgat et al. (1989), Crawford et al. (1999), Tomas et al. (2001) and Le Crâne et al. (2006) required measurements of RO_2 by UV absorption spectroscopy. The convoluted UV signal was fit using predetermined absorption cross-sections and a numerical model simulation, which were likely to add uncertainty as no radical recycling channel was considered. Re-evaluation of the data reported by Tomas et al. (2001) and Le Crâne et al. (2006) by Jenkin et al. (2007) suggested this to be the case. The determination of $k_{(R5)}$ by Dillon and Crowley (2008) relied on the more sensitive and specific LIF detection of OH, however, the calibration of the LIF setup, calculation of HO_2 and RO_2 concentrations and chemical modelling of the system all relied on the determination of $[Cl]_0$ through a Joule meter reading of laser fluence, resulting in the $\pm 30\%$ uncertainty in $k_{(R5)}$ quoted by the authors. This study has been superseded by the determination of $k_{(R5)} = 2.1 \times 10^{-11}\ cm^3\ molecule\ s^{-1}$ – underpinned by direct HO_2 and RO_2 observations, so avoiding this reliance on a Joule meter (Groß et al., 2014a).

3.4.1 Determination of $k_{(R5)}$

Our reported value $k_{(R5)} = (2.4 \pm 0.4) \times 10^{-11}\ cm^3\ molecule^{-1}\ s^{-1}$, is slightly larger than the reported value by Groß et al. (2014a), though within experimental error, and also inside the upper bound quoted in the IUPAC recommendation ($k_{(R5)} = (1.4^{+1.4}_{-0.7}) \times 10^{-11}\ cm^3\ molecule^{-1}\ s^{-1}$). Here, $k_{(R5)}$ was determined by measuring all products from

Reaction (R5) directly and using the chemical simulation outlined in Table 2 to fit to the measured data, summing the individual rate coefficients of branching pathways. This procedure relied on the accurate measurement of $CH_3C(O)OOH$ and $CH_3C(O)OH$ by FTIR, O_3 by UV absorption and OH by FAGE, which have been discussed in more detail in Sect. 3.3.3 and the Supplement.

The ratio of the rate coefficients ($k_{(R5a)}/k_{(R5b)}$) can also be used as a metric to compare results. $k_{(R5a)}/k_{(R5b)}$ has been estimated as 3.2 ± 0.2 across the all experiments presented here, which is in agreement with the IUPAC recommendation and others all the way back to the first investigation of the reaction by Niki et al. (1985), which was insensitive to channel (Reaction R5c). The high measurement of $k_{(R5a)}$ by Crawford et al. (1999) was corrected for the $CH_3C(O)OOH$ absorption cross-section by Orlando et al. (2000), calculating $k_{(R5a)}/k_{(R5b)} = 2.6$, in line with other reported values. The preservation of this ratio in the work presented here helps substantiate a higher rate coefficient for Reaction (R5c), although this does not correlate with the more recent study by Groß et al. (2014b), where $k_{(R5a)}/k_{(R5b)} = 1.44$.

Groß et al. (2014b) mentioned that the discrepancy between their results for $k_{(R5a)}/k_{(R5b)}$ and those previously published on longer timescale chamber experiments, insensitive to OH directly, either may have been caused by the relatively large uncertainty on their value of $k_{(R5b)}$. This uncertainty entered twice in the $k_{(R5a)}/k_{(R5b)}$ ratio as $k_{(R5a)}$ was calculated from $k_{(R5b)}$ and $k_{(R5c)}$ assuming only these three reaction channels of Reaction (R5). In fact they could show that their data would, within the experimental uncertainty, also support a $k_{(R5a)}/k_{(R5b)}$ ratio of 3 and the effects of this are discussed in the following section. Additionally, Groß et al. pointed out that these discrepancies could as well be due to the fact that in the latter publications $k_{(R5a)}/k_{(R5b)}$ ratios are derived from the $CH_3C(O)OOH$ to $CH_3C(O)OH$ or the $CH_3C(O)OH$ to O_3 ratios. These two ratios would not necessarily have to be identical since $CH_3C(O)OH$ production through reactions such as CH_3O_2 with $CH_3C(O)O_2$ (Reaction R20a), could be competitive with (Reaction R5b), as the $CH_3C(O)OH$ yield is still uncertain ($\alpha_{(R20a)} = 0.1 \pm 0.1$). However, this explanation can now be ruled out since experiments presented

here in an HO_2 deficient regime (i.e. $[CH_3OH]_0 = 0$), suggest that the recommended $CH_3C(O)OH$ yield for the reaction of CH_3O_2 with $CH_3C(O)O_2$ could be reduced from 0.1 to ~ 0.05, although a more thorough investigation into this branching ratio is required.

3.4.2 Determination of the OH yield, $\alpha_{(R5c)}$.

The OH yield, $\alpha_{(R5c)}$, presented here is greater than recommended by the IUPAC data evaluation and in agreement with higher yields given by Dillon and Crowley (2008) and Groß et al. (2014b) The slight underestimation of $\alpha_{(R5c)}$ from previous chamber based experiments compared to the results from direct OH detection could be due to assumptions and estimations made in the complex chemical model used to predict the Reaction (R5c) branching ratio in the previous studies.

Using the results from the Groß et al. (2014b) study ($k_{(R5)} = 2.1 \times 10^{-11}\,cm^3\,molecule^{-1}\,s^{-1}$), yields were assigned to the measured results presented here by adjusting the simulated branching ratios giving $\alpha_{(R5a)} : \alpha_{(R5b)} : \alpha_{(R5c)} = (0.38 \pm 0.08) : (0.12 \pm 0.02) : (0.50 \pm 0.08)$. Our assignments bring the $k_{(R5a)}/k_{(R5b)}$ ratio into agreement with the fitted model results and those from previous studies (3.1 ± 0.3). Groß et al. suggest that adjusting the $\alpha_{(R5a)} = (0.29 \pm 0.03)$ and $\alpha_{(R5b)} = (0.10 \pm 0.03)$ whilst fixing $\alpha_{(R5c)} = (0.61 \pm 0.08)$ would bring their results into agreement, without exceeding the uncertainty bounds of $\alpha_{(R5b)}$. This would still not account for the difference in branching ratios observed here. More interestingly, Groß et al. observed a slight decay in $\alpha_{(R5c)}$ as a function of increase in pressure of their system ($\sim 15\%$ reduction between 133 to 667 mbar). The decrease in $\alpha_{(R5c)}$ from 0.61 ± 0.08 to 0.54 ± 0.08 at 667 mbar could explain our adjustment of $\alpha_{(R5c)} = 0.51 \pm 0.06$ to better fit the data presented here at 1000 mbar. However, limited data were collected at the higher pressures in their experiments and the change was deemed statistically insignificant, leading the authors to quote a pressure independent yield. Previously, Dillon and Crowley (2008) reported a pressure independent yield for $\alpha_{(R5c)}$ also,

however the uncertainty in their measurement encompasses the span of the results presented here and in the Groß et al. study ($\alpha_{(R5c)} = 0.50 \pm 0.20$).

4   Conclusions and atmospheric implications

The experiments presented here were successful in directly measuring yields from all three branching pathways of the reaction of HO_2 with $CH_3C(O)O_2$ for the first time using FAGE coupled to the HIRAC chamber. The observations could only be interpreted using a higher rate constant ($k_{(R5)} = (2.4 \pm 0.4) \times 10^{-11}\,cm^3\,molecule^{-1}\,s^{-1}$) for the title reaction than the current IUPAC recommendation. This result is in good agreement with a recent experimental result from Groß et al. (2014b) obtained by complementary methods. Considering the large experimental uncertainty associated with earlier determinations, (Sect. 3.4), we recommend an overall rate coefficient of $k_{(R5)} = (2.2 \pm 0.5) \times 10^{-11}\,cm^3\,molecule^{-1}\,s^{-1}$ at around ambient temperature. This value, based on the results of this work and Groß et al. is within the upper range of the error bar for the IUPAC evaluation and considerably reduces the uncertainty in this important parameter. The branching ratios obtained in this work: $\alpha_{(R5a)} = 0.37 \pm 0.10$, $\alpha_{(R5b)} = 0.12 \pm 0.04$ and $\alpha_{(R5c)} = 0.51 \pm 0.12$ indicate that OH recycling via Reaction (R5) is more rapid than previously thought.

We investigate the global impact of the updated rate constant and yields using the GEOS-Chem (v9.02 $4° \times 5°$ resolution) (Bey et al., 2001; Parrella et al., 2012) tropospheric chemistry transport model. Figure 8a shows the fractional change in surface OH concentrations from a model simulation using the rate coefficient and branching ratios from this work in comparison with same overall rate coefficient and ratio of $k_{(R5a)}:k_{(R5b)}$ but with the OH channel set to zero. It can be seen that there is a significant increase in OH levels over forested tropical areas (up to 11 %), similar to that modelled in an earlier study by Lelieveld et al. (2008) demonstrating the significance of this process. Figure 8b shows the effect of the current rate coefficients and branching ratios in comparison to the IUPAC recommended

F. A. F. Winiberg et al.

Title Page

Abstract | Introduction

Conclusions | References

Tables | Figures

|◄ | ►|

◄ | ►

Back | Close

Full Screen / Esc

Printer-friendly Version

Interactive Discussion

values. The enhancements here are less dramatic as IUPAC already recommended a significant OH yield, but an increase of up to 5 % is observed over parts of the Amazon region.

There is also in increase in OH concentrations at equatorial latitudes at an altitude of 6–8 km (see Supplement) of ∼ 10 % compared to the IUPAC recommended rate coefficients and yields. The RO$_2$ + HO$_2$ reaction could therefore play an important role in OH recycling in the upper troposphere, however to date no temperature dependent studies into the OH yield from substituted RO$_2$ + HO$_2$ radical reactions exist. Additional temperature dependent studies would also provide insights into the mechanism of Reaction (R5). The theoretical studies of Le Crâne et al. (2006) and Hasson et al. (2005) suggest that the exothermicity of channel (Reaction R5c) is small and hence one might expect to see significant temperature dependence in the yield distribution.

Only very slight increases in O$_3$ are observed (see Supplement) as the reaction is only significant when NO concentration are low as so O$_3$ production is low. The enhanced rate coefficients for Reaction (R5) of this work and of Groß et al. (2014a, b) have a significant effect on PAN concentrations as it leads to faster destruction of the peroxy-acetyl radical in the atmosphere. This leads to up to a 30 % reduction in PAN and hence in background NO$_x$ in remote environments as shown in Fig. 9a and b. In these plots the comparison is between the branching ratios and rate coefficients of this work and the IUPAC recommendations. Further comparisons, including vertical profiles, can be found in the Supplement.

The Supplement contains information on: characterisation of HIRAC lamps, further examples of experimental data, details of investigations into possible interferences and outputs from GEOS-Chem modelling.

The Supplement related to this article is available online at doi:10.5194/acpd-15-28815-2015-supplement.

References

Atkinson, R., Baulch, D. L., Cox, R. A., Crowley, J. N., Hampson, R. F., Hynes, R. G., Jenkin, M. E., Rossi, M. J., and Troe, J.: Evaluated kinetic and photochemical data for atmospheric chemistry: Volume I – gas phase reactions of O_x, HO_x, NO_x and SO_x species, Atmos. Chem. Phys., 4, 1461–1738, doi:10.5194/acp-4-1461-2004, 2004.

Atkinson, R., Baulch, D. L., Cox, R. A., Crowley, J. N., Hampson, R. F., Hynes, R. G., Jenkin, M. E., Rossi, M. J., Troe, J., and IUPAC Subcommittee: Evaluated kinetic and photochemical data for atmospheric chemistry: Volume II – gas phase reactions of organic species, Atmos. Chem. Phys., 6, 3625–4055, doi:10.5194/acp-6-3625-2006, 2006.

Atkinson, R., Baulch, D. L., Cox, R. A., Crowley, J. N., Hampson, R. F., Hynes, R. G., Jenkin, M. E., Rossi, M. J., and Troe, J.: Evaluated kinetic and photochemical data for atmospheric chemistry: Volume III – gas phase reactions of inorganic halogens, Atmos. Chem. Phys., 7, 981–1191, doi:10.5194/acp-7-981-2007, 2007.

Atkinson, R., Baulch, D. L., Cox, R. A., Crowley, J. N., Hampson, R. F., Hynes, R. G., Jenkin, M. E., Rossi, M. J., Troe, J., and Wallington, T. J.: Evaluated kinetic and photochemical data for atmospheric chemistry: Volume IV – gas phase reactions of organic halogen species, Atmos. Chem. Phys., 8, 4141–4496, doi:10.5194/acp-8-4141-2008, 2008.

Barnes, I., Becker, K. H., Fink, E. H., Reimer, A., Zabel, F., and Niki, H.: FTIR spectroscopic study of the gas-phase reaction of HO_2 with H_2CO, Chem. Phys. Lett., 115, 1–8, doi:10.1016/0009-2614(85)80091-9, 1985.

Bey, I., Jacob, D. J., Yantosca, R. M., Logan, J. A., Field, B. D., Fiore, A. M., Li, Q. B., Liu, H. G. Y., Mickley, L. J., and Schultz, M. G.: Global modeling of tropospheric chemistry with assimilated meteorology: Model description and evaluation, J. Geophys. Res.-Atmos., 106, 23073–23095, doi:10.1029/2001jd000807, 2001.

Title Page

Abstract | Introduction

Conclusions | References

Tables | Figures

|◀ | ▶|

◀ | ▶

Back | Close

Full Screen / Esc

Printer-friendly Version

Interactive Discussion

Bossolasco, A., Farago, E. P., Schoemaecker, C., and Fittschen, C.: Rate constant of the reaction between CH_3O_2 and OH radicals, Chem. Phys. Lett., 593, 7–13, doi:10.1016/j.cplett.2013.12.052, 2014.

Carslaw, N., Creasey, D. J., Harrison, D., Heard, D. E., Hunter, M. C., Jacobs, P. J., Jenkin, M. E., Lee, J. D., Lewis, A. C., Pilling, M. J., Saunders, S. M., and Seakins, P. W.: OH and HO_2 radical chemistry in a forested region of north-western Greece, Atmos. Environ., 35, 4725–4737, 2001.

Crawford, M. A., Wallington, T. J., Szente, J. J., Maricq, M. M., and Francisco, J. S.: Kinetics and mechanism of the acetylperoxy plus HO_2 reaction, J. Phys. Chem. A, 103, 365–378, doi:10.1021/Jp983150t, 1999.

Dillon, T. J. and Crowley, J. N.: Direct detection of OH formation in the reactions of HO_2 with $CH_3C(O)O_2$ and other substituted peroxy radicals, Atmos. Chem. Phys., 8, 4877–4889, doi:10.5194/acp-8-4877-2008, 2008.

Fittschen, C., Whalley, L. K., and Heard, D. E.: The reaction of CH_3O_2 radicals with OH radicals: a neglected sink for CH_3O_2 in the remote atmosphere, Environ. Sci. Technol., 48, 7700–7701, doi:10.1021/es502481q, 2014.

Fuchs, H., Bohn, B., Hofzumahaus, A., Holland, F., Lu, K. D., Nehr, S., Rohrer, F., and Wahner, A.: Detection of HO_2 by laser-induced fluorescence: calibration and interferences from RO_2 radicals, Atmos. Meas. Tech., 4, 1209–1225, doi:10.5194/amt-4-1209-2011, 2011.

Glowacki, D. R., Goddard, A., Hemavibool, K., Malkin, T. L., Commane, R., Anderson, F., Bloss, W. J., Heard, D. E., Ingham, T., Pilling, M. J., and Seakins, P. W.: Design of and initial results from a highly instrumented reactor for atmospheric chemistry (HIRAC), Atmos. Chem. Phys., 7, 5371–5390, doi:10.5194/acp-7-5371-2007, 2007a.

Glowacki, D. R., Goddard, A., and Seakins, P. W.: Design and performance of a throughput-matched, zero-geometric-loss, modified three objective multipass matrix system for FTIR spectrometry, Appl. Optics, 46, 7872–7883, 2007b.

Groß, C. B. M., Dillon, T. J., and Crowley, J. N.: Pressure dependent OH yields in the reactions of CH_3CO and $HOCH_2CO$ with O_2, Phys. Chem. Chem. Phys., 16, 10990–10998, doi:10.1039/c4cp01108b, 2014a.

Groß, C. B. M., Dillon, T. J., Schuster, G., Lelieveld, J., and Crowley, J. N.: Direct kinetic study of OH and O_3 formation in the reaction of $CH_3C(O)O_2$ with HO_2, J. Phys. Chem. A, 118, 974–985, doi:10.1021/jp412380z, 2014b.

Hasson, A. S., Tyndall, G. S., and Orlando, J. J.: A product yield study of the reaction of HO_2 radicals with ethyl peroxy, acetyl peroxy and acetonyl peroxy radicals, J. Phys. Chem. A, 108, 5979–5989, 2004.

Hasson, A. S., Kuwata, K. T., Arroyo, M. C., and Petersen, E. B.: Theoretical studies of the reaction of hydroperoxy radicals (HO_2) with ethyl peroxy ($CH_3CH_2O_2$), acetyl peroxy ($CH_3C(O)O_2$) and acetonyl peroxy ($CH_3C(O)CH_2O_2$) radicals, J. Photoch. Photobio. A, 176, 218–230, doi:10.1016/j.jphotochem.2005.08.012, 2005.

Hofzumahaus, A., Rohrer, F., Lu, K. D., Bohn, B., Brauers, T., Chang, C. C., Fuchs, H., Holland, F., Kita, K., Kondo, Y., Li, X., Lou, S. R., Shao, M., Zeng, L. M., Wahner, A., and Zhang, Y. H.: Amplified trace gas removal in the troposphere, Science, 324, 1702–1704, doi:10.1126/science.1164566, 2009.

Horie, O. and Moortgat, G. K.: Reactions of $CH_3C(O)O_2$ radicals with CH_3O_2 and HO_2 between 263 and 333,K – a product study, J. Chem. Soc. Faraday T., 88, 3305–3312, doi:10.1039/Ft9928803305, 1992.

Jenkin, M. E., Hurley, M. D., and Wallington, T. J.: Investigation of the radical product channel of the $CH_3C(O)O_2 + HO_2$ reaction in the gas phase, Phys. Chem. Chem. Phys., 9, 3149–3162, doi:10.1039/b702757e, 2007.

Kintecus: Windows Version 2.80, available at: www.kintecus.com, last access: 30 May 2015, 2002.

Kleindienst, T. E., Hudgens, E. E., Smith, D. F., McElroy, F. F., and Bufalini, J. J.: Comparison of chemiluminescence and ultraviolet ozone monitor responses in the presence of humidity and photochemical pollutants, JAPCA J. Air Waste Ma., 43, 213–222, 1993.

Kwok, E. S. C. and Atkinson, R.: Estimation of hydroxyl radical reaction rate constants for gas-phase organiccompounds using a structure–reactivity relationship – an update, Atmos. Environ., 29, 1685–1695, 1995.

Le Crâne, J. P., Rayez, M. T., Rayez, J. C., and Villenave, E.: A reinvestigation of the kinetics and the mechanism of the $CH_3C(O)O_2 + HO_2$ reaction using both experimental and theoretical approaches, Phys. Chem. Chem. Phys., 8, 2163–2171, doi:10.1039/b518321a, 2006.

Lee, M. H., Heikes, B. G., and O'Sullivan, D. W.: Hydrogen peroxide and organic hydroperoxide in the troposphere: a review, Atmos. Environ., 34, 3475–3494, doi:10.1016/S1352-2310(99)00432-X, 2000.

Lelieveld, J., Butler, T. M., Crowley, J. N., Dillon, T. J., Fischer, H., Ganzeveld, L., Harder, H., Lawrence, M. G., Martinez, M., Taraborrelli, D., and Williams, J.: Atmospheric oxidation

Direct measurements of OH and other product yields from the $HO_2 + CH_3C(O)O_2$ reaction

F. A. F. Winiberg et al.

Title Page

Abstract	Introduction
Conclusions	References
Tables	Figures

|◄ | ►|

◄ | ►

Back | Close

Full Screen / Esc

Printer-friendly Version

Interactive Discussion

capacity sustained by a tropical forest, Nature, 452, 737–740, doi:10.1038/nature06870, 2008.

Lightfoot, P. D., Cox, R. A., Crowley, J. N., Destriau, M., Hayman, G. D., Jenkin, M. E., Moortgat, G. K., and Zabel, F.: Organic peroxy-radicals – kinetics, spectroscopy and tropospheric chemistry, Atmos. Environ., 26, 1805–1961, 1992.

Lou, S., Holland, F., Rohrer, F., Lu, K., Bohn, B., Brauers, T., Chang, C.C., Fuchs, H., Häseler, R., Kita, K., Kondo, Y., Li, X., Shao, M., Zeng, L., Wahner, A., Zhang, Y., Wang, W., and Hofzumahaus, A.: Atmospheric OH reactivities in the Pearl River Delta – China in summer 2006: measurement and model results, Atmos. Chem. Phys., 10, 11243–11260, doi:10.5194/acp-10-11243-2010, 2010.

Malkin, T. L., Goddard, A., Heard, D. E., and Seakins, P. W.: Measurements of OH and HO_2 yields from the gas phase ozonolysis of isoprene, Atmos. Chem. Phys., 10, 1441–1459, doi:10.5194/acp-10-1441-2010, 2010.

Mao, J., Ren, X., Zhang, L., Van Duin, D. M., Cohen, R. C., Park, J.-H., Goldstein, A. H., Paulot, F., Beaver, M. R., Crounse, J. D., Wennberg, P. O., DiGangi, J. P., Henry, S. B., Keutsch, F. N., Park, C., Schade, G. W., Wolfe, G. M., Thornton, J. A., and Brune, W. H.: Insights into hydroxyl measurements and atmospheric oxidation in a California forest, Atmos. Chem. Phys., 12, 8009–8020, doi:10.5194/acp-12-8009-2012, 2012.

Moortgat, G. K., Veyret, B., and Lesclaux, R.: Kinetics of the reaction of HO_2 with $CH_3C(O)O_2$ in the temperature range 253–368,K, Chem. Phys. Lett., 160, 443–447, 1989.

Niki, H., Maker, P. D., Savage, C. M., and Breitenbach, L. P.: FTIR study of the kinetics and mechanism for chlorine-atom-initiated reactions of acetaldehyde, J. Phys. Chem., 89, 588–591, 1985.

Novelli, A., Hens, K., Tatum Ernest, C., Kubistin, D., Regelin, E., Elste, T., Plass-Dülmer, C., Martinez, M., Lelieveld, J., and Harder, H.: Characterisation of an inlet pre-injector laser-induced fluorescence instrument for the measurement of atmospheric hydroxyl radicals, Atmos. Meas. Tech., 7, 3413–3430, doi:10.5194/amt-7-3413-2014, 2014.

Orlando, J. J. and Tyndall, G. S.: Gas phase UV absorption spectra for peracetic acid, and for acetic acid monomers and dimers, J. Photoch. Photobio. A, 157, 161–166, doi:10.1016/s1010-6030(03)00067-4, 2003.

Orlando, J. J. and Tyndall, G. S.: Laboratory studies of organic peroxy radical chemistry: an overview with emphasis on recent issues of atmospheric significance, Chem. Soc. Rev., 41, 6294–6317, doi:10.1039/c2cs35166h, 2012.

Title Page

Abstract | Introduction

Conclusions | References

Tables | Figures

|◄ | ►|

◄ | ►

Back | Close

Full Screen / Esc

Printer-friendly Version

Interactive Discussion

Orlando, J. J., Tyndall, G. S., Vereecken, L., and Peeters, J.: The atmospheric chemistry of the acetonoxy radical, J. Phys. Chem. A, 104, 11578–11588, doi:10.1021/Jp0026991, 2000.

Parrella, J. P., Jacob, D. J., Liang, Q., Zhang, Y., Mickley, L. J., Miller, B., Evans, M. J., Yang, X., Pyle, J. A., Theys, N., and Van Roozendael, M.: Tropospheric bromine chemistry: implications for present and pre-industrial ozone and mercury, Atmos. Chem. Phys., 12, 6723–6740, doi:10.5194/acp-12-6723-2012, 2012.

Paulot, R., Crounse, J. D., Kjaergaard, H. G., Kurten, A., St. Clair, J. M., Seinfeld, J. H., and Wennberg, P. O.: Unexpected epoxide formation in the gas-phase photooxidation of isoprene, Science, 325, 730–733, 2009.

Peeters, J. and Muller, J. F.: HO_x radical regeneration in isoprene oxidation via peroxy radical isomerisations, II: experimental evidence and global impact, Phys. Chem. Chem. Phys., 12, 14227–14235, doi:10.1039/c0cp00811g, 2010.

Peeters, J., Nguyen, T. L., and Vereecken, L.: HO_x radical regeneration in the oxidation of isoprene, Phys. Chem. Chem. Phys., 11, 5935–5939, 2009.

Phillips, G. J., Pouvesle, N., Thieser, J., Schuster, G., Axinte, R., Fischer, H., Williams, J., Lelieveld, J., and Crowley, J. N.: Peroxyacetyl nitrate (PAN) and peroxyacetic acid (PAA) measurements by iodide chemical ionisation mass spectrometry: first analysis of results in the boreal forest and implications for the measurement of PAN fluxes, Atmos. Chem. Phys., 13, 1129–1139, doi:10.5194/acp-13-1129-2013, 2013.

Press, W., Teukolsky, S., Vetterling, W., and Flannery, B.: Numerical Recipes in C (2nd Edn.): The Art of Scientific Computing, Cambridge University Press, Cambridge, 1992.

Pugh, T. A. M., MacKenzie, A. R., Hewitt, C. N., Langford, B., Edwards, P. M., Furneaux, K. L., Heard, D. E., Hopkins, J. R., Jones, C. E., Karunaharan, A., Lee, J., Mills, G., Misztal, P., Moller, S., Monks, P. S., and Whalley, L. K.: Simulating atmospheric composition over a South-East Asian tropical rainforest: performance of a chemistry box model, Atmos. Chem. Phys., 10, 279–298, doi:10.5194/acp-10-279-2010, 2010.

Rohrer, F. and Berresheim, H.: Strong correlation between levels of tropospheric hydroxyl radicals and solar ultraviolet radiation, Nature, 442, 184–187, doi:10.1038/Nature04924, 2006.

Sander, S. P., Friedl, R. R., Abbatt, J. P. D., Barker, J., Golden, D. M., Kolb, C. E., Kurylo, M. J., Moortgat, G. K., Wine, P. H., Huie, R. E., and Orkin, V. L.: Chemical kinetics and photochemical data for use in atmospheric studies – Evaluation No. 17, JPL Publication 10-6, available at: http://jpldataeval.jpl.nasa.gov/, last access: 30 May 2015, 2011.

Title Page

Abstract | Introduction

Conclusions | References

Tables | Figures

|◄ | ►|

◄ | ►

Back | Close

Full Screen / Esc

Printer-friendly Version

Interactive Discussion

Saunders, S. M., Jenkin, M. E., Derwent, R. G., and Pilling, M. J.: Protocol for the development of the Master Chemical Mechanism, MCM v3 (Part A): tropospheric degradation of non-aromatic volatile organic compounds, Atmos. Chem. Phys., 3, 161–180, doi:10.5194/acp-3-161-2003, 2003.

Seakins, P. W., Orlando, J. J., and Tyndall, G. S.: The rate coefficients and fraction of vibrationally excited HCl from the reactions of chlorine atoms with methanol, ethanol, acetaldehyde and formaldehyde., Phys. Chem. Chem. Phys., 6, 2224–2229, 2004.

Stone, D., Whalley, L. K., and Heard, D. E.: Tropospheric OH and HO_2 radicals: field measurements and model comparisons, Chem. Soc. Rev., 41, 6348–6404, doi:10.1039/c2cs35140d, 2012.

Taraborrelli, D., Lawrence, M. G., Butler, T. M., Sander, R., and Lelieveld, J.: Mainz Isoprene Mechanism 2 (MIM2): an isoprene oxidation mechanism for regional and global atmospheric modelling, Atmos. Chem. Phys., 9, 2751–2777, doi:10.5194/acp-9-2751-2009, 2009.

Taraborrelli, D., Lawrence, M. G., Crowley, J. N., Dillon, T. J., Gromov, S., Gross, C. B. M., Vereecken, L., and Lelieveld, J.: Hydroxyl radical buffered by isoprene oxidation over tropical forests, Nat. Geosci., 5, 190–193, doi:10.1038/ngeo1405, 2012.

Tomas, A., Villenave, E., and Lesclaux, R.: Reactions of the HO_2 radical with CH_3CHO and $CH_3C(O)O_2$ in the gas phase, J. Phys. Chem. A, 105, 3505–3514, 2001.

Tyndall, G. S., Cox, R. A., Granier, C., Lesclaux, R., Moortgat, G. K., Pilling, M. J., Ravishankara, A. R., and Wallington, T. J.: Atmospheric chemistry of small organic peroxy radicals, J. Geophys. Res.-Atmos., 106, 12157–12182, 2001.

Veyret, B., Lesclaux, R., Rayez, M. T., Rayez, J. C., Cox, R. A., and Moortgat, G. K.: Kinetics and mechanism of the photo-oxidation of formaldehyde., 1. flash photolysis study, J. Phys. Chem., 93, 2368–2374, 1989.

Wayne, R. P.: Chemistry of atmospheres: an introduction to the chemistry of the atmospheres of Earth, the planets, and their satellites, 2nd edn., Clarendon, Oxford, 1991.

Whalley, L. K., Edwards, P. M., Furneaux, K. L., Goddard, A., Ingham, T., Evans, M. J., Stone, D., Hopkins, J. R., Jones, C. E., Karunaharan, A., Lee, J. D., Lewis, A. C., Monks, P. S., Moller, S. J., and Heard, D. E.: Quantifying the magnitude of a missing hydroxyl radical source in a tropical rainforest, Atmos. Chem. Phys., 11, 7223–7233, doi:10.5194/acp-11-7223-2011, 2011.

Whalley, L. K., Blitz, M. A., Desservettaz, M., Seakins, P. W., and Heard, D. E.: Reporting the sensitivity of laser-induced fluorescence instruments used for HO_2 detection to an

interference from RO_2 radicals and introducing a novel approach that enables HO_2 and certain RO_2 types to be selectively measured, Atmos. Meas. Tech., 6, 3425–3440, doi:10.5194/amt-6-3425-2013, 2013.

Winiberg, F. A. F.: Characterisation of FAGE apparatus for HO_x detection and application in an environmental chamber, PhD, School of Chemistry, University of Leeds, Leeds, 232 pp., 2014.

Winiberg, F. A. F., Smith, S. C., Bejan, I., Brumby, C. A., Ingham, T., Malkin, T. L., Orr, S. C., Heard, D. E., and Seakins, P. W.: Pressure-dependent calibration of the OH and HO_2 channels of a FAGE HO_x instrument using the Highly Instrumented Reactor for Atmospheric Chemistry (HIRAC), Atmos. Meas. Tech., 8, 523–540, doi:10.5194/amt-8-523-2015, 2015.

Wolfe, G. M., Crounse, J. D., Parrish, J. D., Clair, J. M. S., Beaver, M. R., Paulot, F., Yoon, T. P., Wennberg, P. O., and Keutsch, F. N.: Photolysis, OH reactivity and ozone reactivity of a proxy for isoprene-derived hydroperoxyenals (HPALDs), Phys. Chem. Chem. Phys., 14, 7276–7286, 2012.

Direct measurements of OH and other product yields from the HO_2 + $CH_3C(O)O_2$ reaction

F. A. F. Winiberg et al.

Title Page

Abstract	Introduction
Conclusions	References
Tables	Figures

|◄ ►|

◄ ►

Back | Close

Full Screen / Esc

Printer-friendly Version

Interactive Discussion

Table 1. Experimental conditions and for the investigation into CH$_3$C(O)O$_2$ + HO$_2$ (Reaction R5) conducted in a synthetic air mixture at 1000 mbar and 293 K. Lower j(Cl$_2$) for experiments P9–P12 due to degradation of lamps over time in between first P1–P8 experiments. Taken from chemical simulation (Sect. 2.4) at close to t = 0 s, units in 10^6 molecule cm^{-3}.

Expt[a]	[Cl$_2$]$_0$[b]	[CH$_3$OH]$_0$[b]	[CH$_3$CHO]$_0$[b]	Ratio[c]	Lamps	j(Cl$_2$)[d]	[Cl]$_0$[e]	Notes
P1	5.89	3.01	0.90	3.3	2	1.25	7.1	
P2	6.51	3.00	0.81	3.7	2	1.25	8.0	
P3	6.08	3.16	0.80	4.0	2	1.25	7.2	
P4	2.21	3.03	0.79	3.8	4	2.50	5.1	No HO$_2$
P5	2.47	3.22	0.79	4.1	8	5.00	11.2	No HO$_2$
P6	6.36	4.02	0.72	5.6	2	1.25	5.8	No O$_3$, no HO$_2$
P7	6.78	0.86	0.56	1.5	2	1.25	11.1	No O$_3$
P8	7.00	0.00	0.70	0.0	2	1.25	20.1	
P9	5.59	0.00	0.73	0.0	2	0.80	17.0	GC
P10	5.79	0.72	0.74	1.0	2	0.80	11.4	GC, no HO$_2$
P11	5.67	2.37	0.69	3.4	2	0.80	5.6	GC, no HO$_2$
P12	2.37	2.65	0.73	3.6	8	3.80	9.9	

[a] All experiments performed at 1000 mbar.
[b] Precursor concentrations in 10^{14} molecule cm^{-3}.
[c] Ratio of [CH$_3$OH]$_0$: [CH$_3$CHO]$_0$.
[d] Photolysis rate units 10^{-4} s^{-1}.
[e] Peak initial Cl atom concentration.

Table 2. Reaction scheme used in the determination of branching ratios for the reaction of CH$_3$C(O)O$_2$ with HO$_2$. RO radical decomposition and reaction with O$_2$ are assumed instantaneous, indicated by (+O$_2$) where appropriate. Rate coefficients sourced from IUPAC recommended values unless otherwise stated, all quoted in units = molecule^{-1} cm^3 s^{-1}. (Atkinson et al., 2004). (a) from (Crawford et al., 1999); (b) estimations from (Jenkin et al., 2007), based on reactivity of Cl with other species containing -OOH, -OH, -CHO functional groups; (c) from (Jenkin et al., 2007), estimation based on the reactivity of -OOH in CH$_3$OOH; (d) taken from Jenkin et al. (2007), estimated based on SAR by (Kwok and Atkinson, 1995) and (Saunders et al., 2003) ; (e) from (Tomas et al., 2001); (f) estimations from (Jenkin et al., 2007), based on analogous reaction for similar α-hydroxy peroxy radicals; (g) estimations from (Jenkin et al., 2007), assumed equivalent to CH$_3$C(O)O$_2$ + CH$_3$O$_2$; (h) estimations from (Jenkin et al., 2007), based on the geometric mean of self-reaction rate coefficients and branching ratios of participating RO$_2$.

	Reaction	Branching Ratio	Rate Coefficient	
	Chlorine Initiation			
R6	Cl$_2$ + h$\nu \rightarrow$ 2Cl		Varied. See text.	
R7,8	Cl + CH$_3$OH(+O$_2$) $\rightarrow$ HCHO + HO$_2$ + HCl		5.5×10^{-11}	
R9,10	Cl + CH$_3$CHO(+O$_2$) $\rightarrow$ CH$_3$C(O)O$_2$ + HCl		8.0×10^{-11}	
R21	Cl + HCHO(+O$_2$) $\rightarrow$ CO + HO$_2$ + HCl		8.1×10^{-11} exp$(-34/T)$	
	Cl reactions			
	Cl + CH$_3$C(O)OOH $\rightarrow$ CH$_3$C(O)O$_2$ + HCl		4.5×10^{-15}	(a)
	Cl + CH$_3$C(O)OH(+O$_2$) $\rightarrow$ CH$_3$O$_2$ + CO$_2$ + HCl		2.65×10^{-14}	
	Cl + H$_2$O$_2$ $\rightarrow$ HO$_2$ + HCl		1.1×10^{-11} exp$(-980/T)$	
	Cl + CH$_3$OOH $\rightarrow$ HCHO + OH + HCl		5.9×10^{-11}	
	Cl + HCOOH(+O$_2$) $\rightarrow$ CO$_2$ + HO$_2$ + HCl		1.9×10^{-13}	
R15,R16	Cl + HOCH$_2$OOH $\rightarrow$ HCOOH + OH + HCl		1.0×10^{-10}	(b)
	Cl + HOCH$_2$OH(+O$_2$) $\rightarrow$ HCOOH + HO$_2$ + HCl		1.0×10^{-10}	(b)
	Cl + CH$_3$CH(OH)OOH $\rightarrow$ CH$_3$C(O)OH + OH + HCl		1.0×10^{-10}	(b)
	Cl + CH$_3$CH(OH)$_2$(+O$_2$) $\rightarrow$ CH$_3$C(O)OH + HO$_2$ + HCl		1.0×10^{-10}	(b)
	Cl + O$_3$ $\rightarrow$ ClO + O$_2$		2.8×10^{-11} exp$(-250/T)$	
	ClO + HO$_2$ $\rightarrow$ HOCl + O$_2$		2.2×10^{-12} exp$(340/T)$	
	Cl + HO$_2$ $\rightarrow$ HCl + O$_2$	0.80	4.4×10^{-11}	
	$\rightarrow$ ClO + OH	0.20		

Table 2. Continued.

	Reaction	Branching Ratio	Rate Coefficient	
	OH reactions			
	$OH + HO_2 \rightarrow H_2O + O_2$		$4.8 \times 10^{-11}\, exp(250/T)$	
	$OH + CH_3C(O)OH \rightarrow CH_3O_2 + CO_2 + H_2O$		$4.2 \times 10^{-14}\, exp(855/T)$	
	$OH + CH_3C(O)OOH \rightarrow CH_3C(O)O_2 + H_2O$		3.6×10^{-12}	(c)
	$OH + H_2O_2 \rightarrow HO_2 + H_2O$		$2.9 \times 10^{-12}\, exp(-160/T)$	
	$OH + CH_3OOH \rightarrow CH_3O_2 + HO_2$	0.65	$2.9 \times 10^{-12}\, exp(190/T)$	
	$\rightarrow HCHO + OH + H_2O$	0.35		
	$OH + HCOOH(+O_2) \rightarrow CO_2 + HO_2 + H_2O$		4.5×10^{-13}	
	$OH + HOCH_2OOH \rightarrow HOCH_2O_2 + H_2O$	0.12	3.1×10^{-11}	(d)
	$\rightarrow HCOOH + OH + H_2O$	0.88		
	$OH + HOCH_2OH(+O_2) \rightarrow HCOOH + OH + H_2O$		1.1×10^{-11}	(d)
	$OH + CH_3CH(OH)OOH \rightarrow CH_3C(O)OH + OH + H_2O$		6.0×10^{-11}	(d)
	$OH + CH_3CH(OH)_2(+O_2) \rightarrow CH_3C(O)OH + HO_2 + H_2O$		2.4×10^{-11}	(d)
	$OH + Cl_2 \rightarrow Cl + HOCl$		$3.6 \times 10^{-12}\, exp(-1200/T)$	(a)
	$OH + CO \rightarrow CO_2 + HO_2$		$1.44 \times 10^{-13} + 3.43 \times 10^{-33}\, [M]$	
	$OH + HCl \rightarrow Cl + H_2O$		$1.7 \times 10^{-12}\, exp(-230/T)$	(a)
	$OH + O_3 \rightarrow HO_2 + O_2$		$1.7 \times 10^{-12}\, exp(-940/T)$	
	$OH + CH_3CHO \rightarrow CH_3C(O)O_2 + H_2O$		$4.4 \times 10^{-12}\, exp(365/T)$	
	$OH + CH_3OH \rightarrow HCHO + HO_2 + H_2O$		$2.85 \times 10^{-12}\, exp(-345/T)$	
	$OH + HCHO \rightarrow CO + HO_2 + H_2O$		$5.4 \times 10^{-12}\, exp(135/T)$	
	HO_2 reactions			
	$HO_2 + O_3 \rightarrow OH + O_2$		$2.03 \times 10^{-16} \times (T/300)^{4.57}\, exp(693/T)$	
R17	$HO_2 + CH_3CHO \rightarrow CH_3CH(OH)O_2$		4.4×10^{-14}	(e)
R-17	$CH_3CH(OH)O_2 \rightarrow HO_2 + CH_3CHO$		$2.3 \times 10^{13}\, exp(-6925/T)$	(e)
R11	$HO_2 + HCHO \rightarrow HOCH_2O_2$		$9.7 \times 10^{-15}\, exp(625/T)$	
R-11	$HOCH_2O_2 \rightarrow HO_2 + HCHO$		$2.4 \times 10^{12}\, exp(-7000/T)$	
	$HO_2 + RO_2$ reactions			
	$HO_2 + HO_2 \rightarrow H_2O_2 + O_2$		$2.2 \times 10^{-15}\, exp(600/T) + 1.9 \times 10^{-33}\,[M]\, exp(980/T)$	
R5a	$CH_3C(O)O_2 + HO_2 \rightarrow CH_3C(O)OOH + O_2$		$5.2 \times 10^{-13}\, exp(980/T)$	
R5b	$\rightarrow CH_3C(O)OH + O_3$		(see text for branching)	
R5c	$(+O_2) \rightarrow CH_3O_2 + CO_2 + OH + O_2$			
	$CH_3O_2 + HO_2 \rightarrow CH_3OOH + O_2$	0.90	$3.8 \times 10^{-13}\, exp(780/T)$	
	$\rightarrow HCHO + H_2O + O_2$	0.10		
R12a	$HOCH_2O_2 + HO_2 \rightarrow HOCH_2OOH + O_2$	0.50	$5.6 \times 10^{-15}\, exp(2300/T)$	
R12b	$\rightarrow HCOOH + H_2O + O_2$	0.30		
R12c	$(+O_2) \rightarrow HCOOH + HO_2 + OH + O_2$	0.20		
	$CH_3CH(OH)O_2 + HO_2 \rightarrow CH_3CH(OH)OOH + O_2$	0.50	$5.6 \times 10^{-15}\, exp(2300/T)$	(f)
	$\rightarrow CH_3C(O)OH + H_2O + O_2$	0.30		
	$(+O_2) \rightarrow HCOOH + CH_3O_2 + OH + O_2$	0.20		

Table 2. Continued.

	Reaction	Branching Ratio	Rate Coefficient	
	RO$_2$ self-reactions			
R18,R19	2CH$_3$C(O)O$_2$(+O$_2$) → 2CH$_3$O$_2$ + O$_2$ + CO$_2$		2.9 × 10^{-12} exp(500/T)	
R22b	2CH$_3$O$_2$ → HCHO + CH$_3$OH + O$_2$	0.63	1.03 × 10^{-13} exp(365/T)	
R22a,R23	(+2O$_2$) → 2HCHO + 2HO$_2$ + O$_2$	0.37		
R13a,R14	2HOCH$_2$O$_2$(+2O$_2$) → 2HCOOH + 2HO$_2$ + O$_2$	0.88	5.7 × 10^{-12}	
R13b	→ HCOOH + HOCH$_2$OH + O$_2$	0.12		
	2CH$_3$CH(OH)O$_2$ → CH$_3$C(O)OH + CH$_3$CH(OH)$_2$ + O$_2$	0.12	5.7 × 10^{-12}	(f)
	(+2O$_2$) → 2HCOOH + 2CH$_3$O$_2$ + O$_2$	0.88		
	RO$_2$ + RO$_2$ reactions			
R20b	CH$_3$C(O)O$_2$ + CH$_3$O$_2$ → CH$_3$C(O)OH + HCHO + O$_2$	0.10	2.0 × 10^{-12} exp(500/T)	
R20a	(+2O$_2$) → CH$_3$O$_2$ + CO$_2$ + HCHO + HO$_2$ + O$_2$	0.90		
	CH$_3$C(O)O$_2$ + HOCH$_2$O$_2$ → CH$_3$C(O)OH + HCOOH + O$_2$	0.10	2.0 × 10^{-12} exp(500/T)	(g)
	(+2O$_2$) → CH$_3$O$_2$ + CO$_2$ + HCOOH + HO$_2$ + O$_2$	0.90		
	CH$_3$C(O)O$_2$ + CH$_3$CH(OH)O$_2$ → 2CH$_3$C(O)OH + O$_2$	0.90	2.0 × 10^{-12} exp(500/T)	(g)
	(+2O$_2$) → CH$_3$O$_2$ + CO$_2$ + HCOOH + CH$_3$O$_2$ + O$_2$	0.10		
	CH$_3$O$_2$ + HOCH$_2$O$_2$ → HCHO + HOCH$_2$OH + O$_2$	0.19	1.4 × 10^{-12}	(h)
	→ CH$_3$OH + HCOOH + O$_2$	0.19		
	(+2O$_2$) → HCHO + HCOOH + 2HO$_2$ + O$_2$	0.62		
	CH$_3$O$_2$ + CH$_3$CH(OH)O$_2$ → HCHO + CH$_3$CH(OH)$_2$ + O$_2$	0.19	1.4 × 10^{-12}	(h)
	→ CH$_3$OH + CH$_3$C(O)OH + O$_2$	0.19		
	(+2O$_2$) → HCHO + HO$_2$ + HCOOH + CH$_3$O$_2$ + O$_2$	0.62		
	HOCH$_2$O$_2$ + CH$_3$CH(OH)O$_2$ → HCOOH + CH$_3$CH(OH)$_2$ + O$_2$	0.06	5.7 × 10^{-12}	(h)
	→ HOCH$_2$OH + CH$_3$C(O)OH + O$_2$	0.06		
	(+2O$_2$) → HCOOH + HO$_2$ + HCOOH + CH$_3$O$_2$ + O$_2$	0.88		

Table 3. Branching ratios for Reaction (R5) determined by fitting the chemical model to the experimental data, allowing the chemical simulation to optimise $k_{(R5a)}$, $k_{(R5b)}$ and $k_{(R5c)}$ independently. The total rate coefficient was determined from the fitting procedure also listed $k_{(R5)}$. The bottom row displays average values and calculated standard deviations ($\pm 2\sigma$). All other experiments conducted using 2 photolysis lamps.

Expt	$\alpha_{(R5a)}$	$\alpha_{(R5b)}$	$\alpha_{(R5c)}$	$k_{(R5a)}$	$k_{(R5b)}$	$k_{(R5c)}$[a]	$k_{(R5)}$[a]
P1	0.41	0.13	0.45	7.22	2.30	7.94	17.5
P2	0.35	0.10	0.55	8.58	2.48	13.3	24.3
P3	0.33	0.11	0.56	9.19	3.05	15.3	27.5
P4[b]	0.32	0.10	0.58	9.09	2.87	16.3	28.3
P5[c]	0.34	0.11	0.55	8.48	2.62	13.8	24.9
P11[b]	0.38	0.11	0.50	8.99	2.69	11.8	23.5
P12[b]	0.45	0.15	0.41	8.41	2.79	7.63	18.8
	0.37 ± 0.10	0.12 ± 0.04	0.51 ± 0.12	8.57	2.69	1.23	24 ± 8

[a] Rate coefficient units in 10^{-12} cm^3 molecule^{-1} s^{-1}.
[b] Experiment conducted using 4 photolysis lamps.
[c] Experiment conducted using 8 photolysis lamps.

Table 4. Comparison of the results determined in this study with those present in the literature. Authors are referenced as they appear in the bibliography and tilde symbols indicate where a value was not measured directly. Data previous to (Hasson et al., 2004) had not considered a third branching pathway ($\alpha_{(R5c)}$) but are included here to compare the ratio of $k_{(R5a)}$ and $k_{(R5b)}$ as well as the overall rate constant for $CH_3C(O)O_2 + HO_2$ ($k_{(R5)}$).

Author	$\alpha_{(R5a)}$	$\alpha_{(R5b)}$	$\alpha_{(R5c)}$	$k_{(R5a)}/k_{(R5b)}$	$k_{(R5)}$[a]
This work	0.38 ± 0.08	0.12 ± 0.02	0.50 ± 0.08	3.1 ± 0.3	2.1[b]
fitted $k_{(R5)}$	0.37 ± 0.10	0.12 ± 0.04	0.51 ± 0.12	3.2 ± 0.2	2.4 ± 0.4
Groß et al. (2014b)	0.23 ± 0.12	0.16 ± 0.08	0.61 ± 0.09	1.44	2.1 ± 0.4
Dillon and Crowley (2008)	–	–	0.50 ± 0.20	–	1.4 ± 0.5
Jenkin et al. (2007)	0.38 ± 0.13	0.12 ± 0.04	0.43 ± 0.10	3.16 ± 0.48	(1.4[c])
Le Crâne et al. (2006)	–	0.20 ± 0.01	< 0.1	–	1.50 ± 0.08
Hasson et al. (2004)	0.40 ± 0.16	0.20 ± 0.08	0.40 ± 0.16	2.00 ± 0.57	2.2
Tomas et al. (2001)	–	0.20 ± 0.02	–	–	1.51 ± 0.07
Crawford et al. (1999)	(0.72)[c]	0.12 ± 0.04	–	7.3 (2.6)[d]	4.4 ± 1.6
Horie and Moortgat (1992)	–	–	–	2.7	–
Moortgat et al. (1989)	–	0.33 ± 0.07	–	–	1.3 ± 0.3
Niki et al. (1985)	∼ 0.75	∼ 0.25	–	∼ 3	–
IUPAC (Atkinson et al., 2006)	0.41 ± 0.20	0.15 ± 0.10	0.44 ± 0.20	2.7	1.4 $^{+1.4}_{-0.7}$

[a] Units for $k_{(R5)}$, molecule^{-1} cm^3 s^{-1}.

[b] Analysis conducted using recently reported value for $k_{(R5)}$ from Gross et al., 2014.

[c] Jenkin et al., 2007 assumed k_{R5} as that recommended by IUPAC.

[d] Bracketed data from (Crawford et al., 1999) corrected for erroneous absorption cross section for $CH_3C(O)OOH$ by (Orlando et al., 2000).
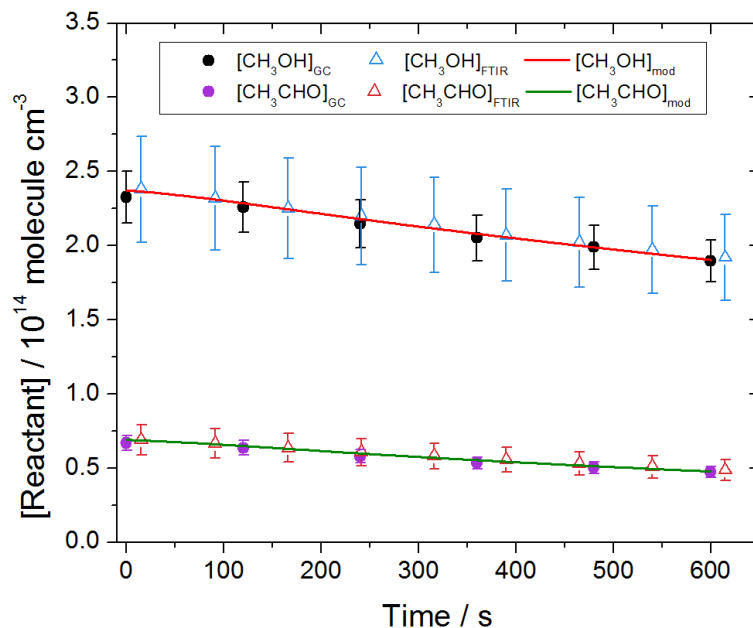
Figure 1. Decay of reactants CH_3CHO and CH_3OH from experiment P11 measured simultaneously using FTIR and GC-FID conducted at 1000 mbar and 298 K. Error bars are representative of the uncertainty in the calibration of the FTIR and GC-FID ($\pm 2\sigma$). Measurements are in excellent agreement within their respective uncertainties. Chemical simulation was conducted using the reaction scheme outlined in Table 2 using $k_{(R5)} = 2.35 \times 10^{-11}\ cm^3\ molecule^{-1}\ s^{-1}$ and $\alpha_{(R5a)} : \alpha_{(R5b)} : \alpha_{(R5c)} = 0.38 : 0.11 : 0.5$. Model concentrations for CH_3CHO and CH_3OH was observed to agree well with the experimental data, confirming accurate prediction of the reactant decays, and therefore the $j(Cl_2)$ photolysis rate ($= (8 \pm 1) \times 10^{-5}\ s^{-1}$).

Title Page

Abstract | Introduction

Conclusions | References

Tables | Figures

|◄ | ►|

◄ | ►
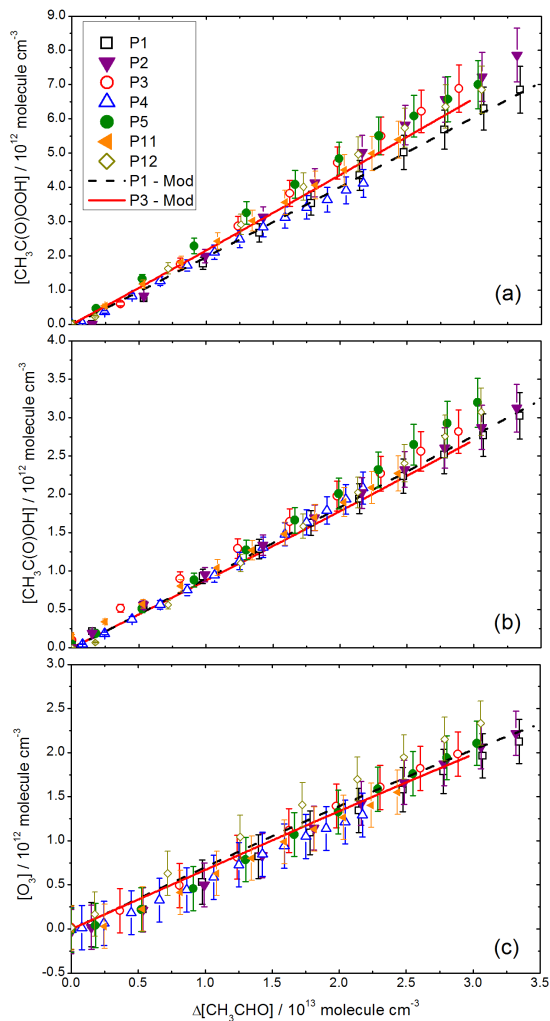
Back | Close

Full Screen / Esc

Printer-friendly Version

Interactive Discussion

Figure 2. Products $CH_3C(O)OOH$, **(a)**, $CH_3C(O)OH$, **(b)**, and O_3, **(c)**, as a function of $\Delta[CH_3CHO]$ for $[CH_3OH]_0 : [CH_3CHO]_0 \approx 4$ in air at 1000 mbar and 293 K for runs P1–P5, P11 and P12. Good agreement was observed between experimental data and the chemical model for all datasets with $k_{(R5)} = 2.4 \times 10^{-11}\ cm^3\ molecule^{-1}\ s^{-1}$ and average determined yields of $\alpha_{(R5a)} = 0.37 \pm 0.10$, $\alpha_{(R5b)} = 0.12 \pm 0.04$ and $\alpha_{(R5c)} = 0.51 \pm 0.12$. Only model runs for experiments P1 and P3 are shown as examples, the optimised branching ratios for which are shown in Table 1. All uncertainties quoted to $\pm 1\sigma$.

Title Page

Abstract | Introduction

Conclusions | References

Tables | Figures

|◀ | ▶|

◀ | ▶

Back | Close

Full Screen / Esc

Printer-friendly Version

Interactive Discussion

OH Production

- $CH_3C(O)O_2+HO_2\rightarrow OH+CO_2+CH_3+O_2$
- $Cl + CH_3OOH\rightarrow OH+HCHO+HCl$
- $HOCH_2O_2+HO_2\rightarrow OH+HCOOH+H+O_2$
- $Cl+HOCH_2O_2\rightarrow OH+HCOOH+HCl$
- $HO_2+O_3\rightarrow OH+2O_2$
- Other

HO₂ Production

- $Cl+CH_3OH+O_2\rightarrow HO_2+HCl+HCHO$
- $Cl+HCHO+O_2\rightarrow HO_2+HCl+CO$
- $CH_3C(O)O_2+CH_3O_2\rightarrow HO_2+products$
- $OH+HCHO+O_2\rightarrow HO_2+CO+H_2O$
- $OH+CH_3OH+O_2\rightarrow HO_2+HCHO+H_2O$
- Other

OH Destruction

- $OH+CH_3CHO\rightarrow CH_3CO+H_2O$
- $OH+CH_3OH\rightarrow CH_2OH+H_2O$
- $OH+HCHO\rightarrow HCO+H_2O$
- Others

HO₂ Destruction

- $HO_2+HO_2\rightarrow H_2O_2+O_2$
- $CH_3C(O)O_2+HO_2\rightarrow products$
- $CH_3O_2+HO_2\rightarrow CH_3OOH+O_2$
- HO_2+HCHO net loss
- $HO_2\rightarrow$ wall loss
- Other

Figure 3. The OH and HO$_2$ time profiles during experiment P1, $[CH_3OH]_0 : [CH_3CHO]_0 \approx$ 4, 1000 mbar in air and 293 K, where photolysis was initiated at $t = 0$ s. Chemical model predictions also shown (solid lines) calculated using optimised branching ratios (P1) $\alpha_{(R5c)} =$ 0.45±0.08 calculated using the fitted $k_{(R5)} = 2.4 \times 10^{-11}$ cm^3 molecule^{-1} s^{-1}. Contribution to total [OH] from Reaction (R5c) and all other secondary sources are shown as dashed and dotted traces respectively. Error bars represent uncertainty to ±1σ in the FAGE calibration procedure. Above and below each profile are shown rate of production and rate of destruction analyses at 120, 300 and 600 s. OH production is dominated by the title reaction and OH loss processes are predominantly controlled by well-characterised reactions. HO$_2$ production and loss is controlled by more reactions, but these too are well-characterised.
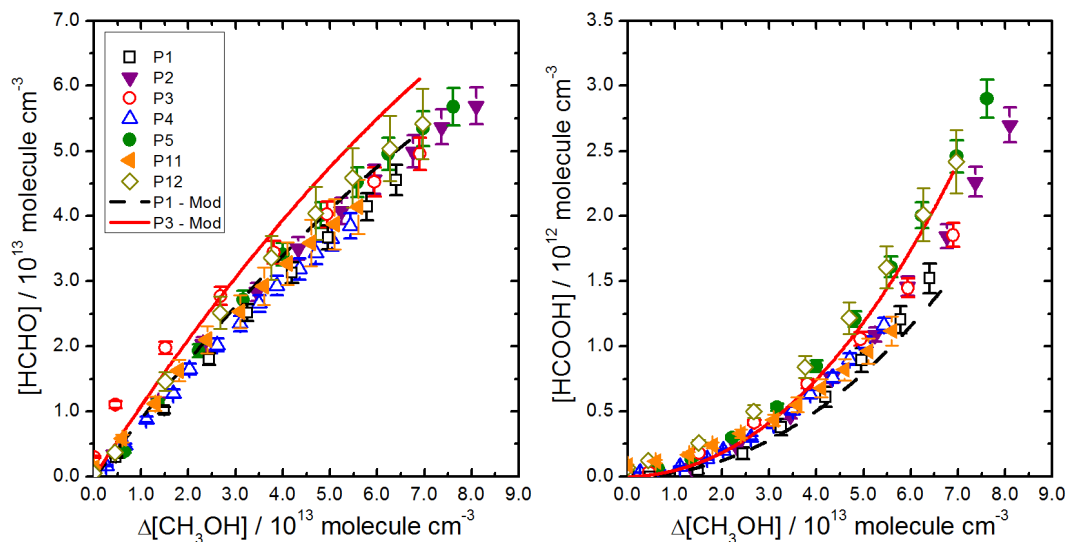
Figure 4. The [HCHO] (left) and [HCOOH] (right) profiles as a function of $\Delta[CH_3OH]$ for experiments P1–P5, P11 and P12, for $[CH_3OH]_0 : [CH_3CHO]_0 \approx 3.8$ at 1000 mbar and 293 K. Good agreement was observed between experimental data and the chemical model for all datasets with $k_{(R5)} = 2.4 \times 10^{-11}$ cm^3 molecule^{-1} s^{-1} and average determined yields of $\alpha_{(R5a)} = 0.37 \pm 0.10$, $\alpha_{(R5b)} = 0.12 \pm 0.04$ and $\alpha_{(R5c)} = 0.51 \pm 0.12$. Only model runs for experiments P1 and P3 are plotted as examples, the optimised (R5) branching ratios for which are shown in Table 1. All uncertainties quoted to $\pm 1\sigma$.
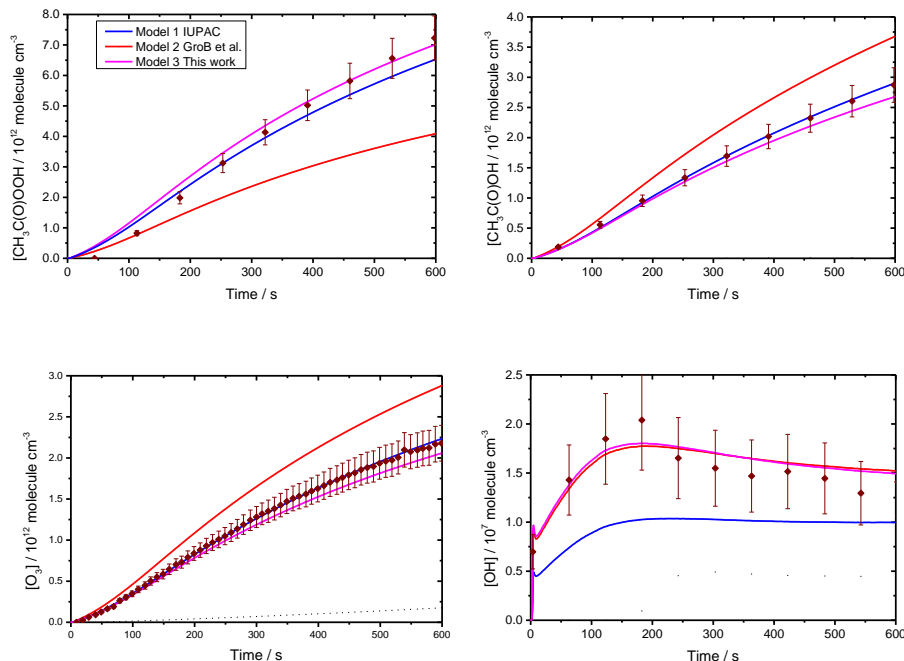
Figure 5. Comparison of the measured $CH_3C(O)OOH$, **(a)**, $CH_3C(O)OH$, **(b)**, O_3, **(c)**, and OH **(d)** with various modelling scenarios, displayed as a function of time for experiment P2 conducted at 1000 mbar and 293 K. Error bars are representative of the uncertainty in the FTIR (for **(a)** − **(c)**) and FAGE **(d)** measurement techniques to ±2σ. Chemical simulations were conducted with different $k_{(R5)}$ and branching ratios $\alpha_{(R5a)} : \alpha_{(R5b)} : \alpha_{(R5c)}$. Model 1 (IUPAC): $k_{(R5)} = 1.4 \times 10^{-11}$ cm^3 molecule^{-1} s^{-1}, $\alpha_{(R5a)} : \alpha_{(R5b)} : \alpha_{(R5c)} = 0.44 : 0.15 : 0.41$. Model 2 (Groß et al., 2014b): $k_{(R5)} = 2.1 \times 10^{-11}$ cm^3 molecule^{-1} s^{-1}, $\alpha_{(R5a)} : \alpha_{(R5b)} : \alpha_{(R5c)} = 0.23 : 0.16 : 0.61$. Model 3 (this work, 2015): $k_{(R5)} = 2.4 \times 10^{-11}$ cm^3 molecule^{-1} s^{-1}, $\alpha_{(R5a)} : \alpha_{(R5b)} : \alpha_{(R5c)} = 0.35 : 0.10 : 0.55$.

Title Page

Abstract | Introduction

Conclusions | References

Tables | Figures

|◄ | ►|

◄ | ►

Back | Close

Full Screen / Esc

Printer-friendly Version

Interactive Discussion
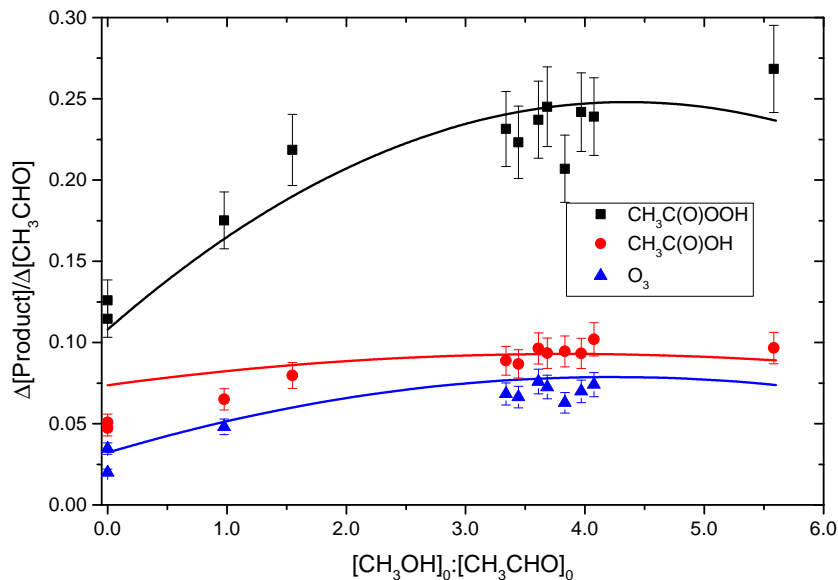
Figure 6. Experimentally determined product yields (relative to decay in CH$_3$CHO) for CH$_3$C(O)OOH, CH$_3$C(O)OH and O$_3$ as a function of the [CH$_3$OH]$_0$: [CH$_3$CHO]$_0$ ratio where each point represents one experiment. Model3 predictions for each species yield also displayed for comparison (solid lines of corresponding colour). Uncertainties calculated to 2σ from linear regression of respective [product] vs. Δ[CH$_3$CHO] plot.
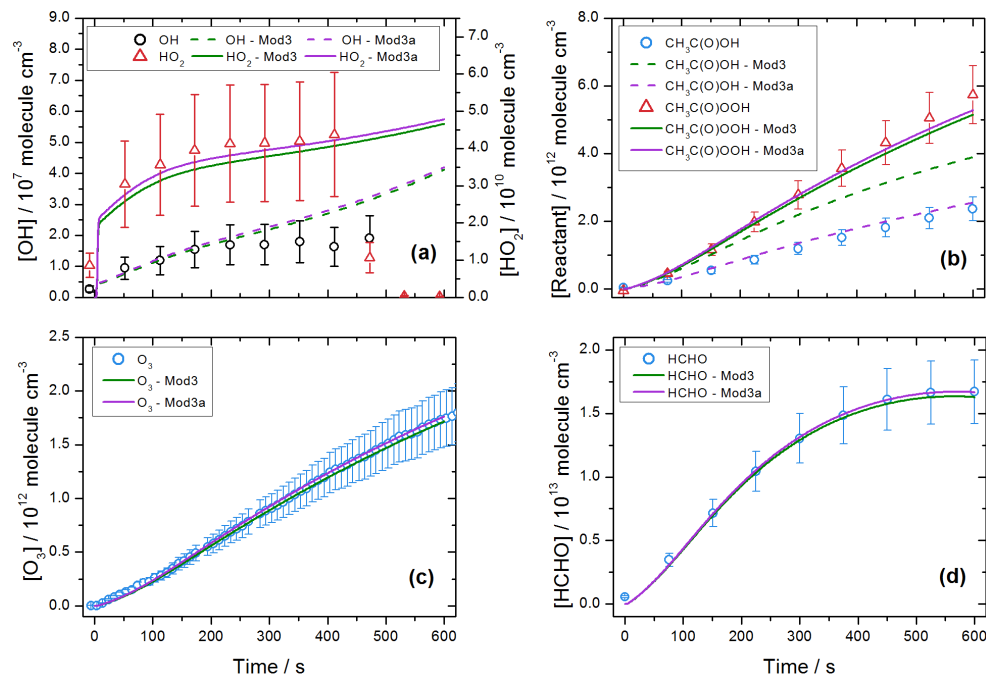
Figure 7. Experimental results for OH and HO$_2$, **(a)**, CH$_3$C(O)OOH and CH$_3$C(O)OH, **(b)**, O$_3$, **(c)** and HCHO, **(d)**, as a function of time for experiment P9 where [CH$_3$OH]$_0$: [CH$_3$CHO]$_0$ = 0.0, 1000 mbar and 293 K. Yields for Reaction (R5) were modelled using the base model reaction scheme shown in Table 2 and varied to fit the measurements, using $k_{(R5)}$ = (2.4 ± 0.4) × 10^{-11} cm^3 molecule^{-1} s^{-1} and $\alpha_{(R5a)}$ = 0.42 ± 0.05, $\alpha_{(R5b)}$ = 0.14 ± 0.04 and $\alpha_{(R5c)}$ = 0.44 ± 0.10 (Model3). Model agreement to measured CH$_3$C(O)OH was improved by varying the modelled branching ratios of Reactions (R20a) and (R20b) are shown in trace Model3a. All uncertainties quoted to ±2σ.
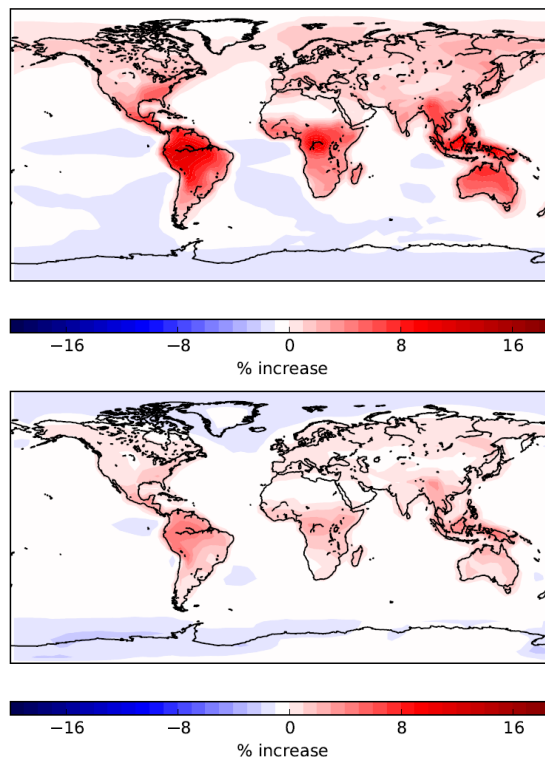
Figure 8. Percentage increase of surface OH concentrations calculated from rate constant and yields from this study ($\alpha_{(R5a)} = 0.37$, $\alpha_{(R5b)} = 0.12$, $\alpha_{(R5c)} = 0.51$, $k_{(R5)} = 2.4 \times 10^{-11}\,\mathrm{cm^3\,molecule^{-1}\,s^{-1}}$) compared to **(a)** the same overall rate coefficient but with the OH channel set to zero ($\alpha_{(R5a)} = 0.75$, $\alpha_{(R5b)} = 0.25$, $\alpha_{(R5c)} = 0$) and with **(b)** the IUPAC recommendation ($\alpha_{(R5a)} = 0.41$, $\alpha_{(R5b)} = 0.15$, $\alpha_{(R5c)} = 0.44$, $k_{(R5)} = 1.4 \times 10^{-11}\,\mathrm{cm^3\,molecule^{-1}\,s^{-1}}$).
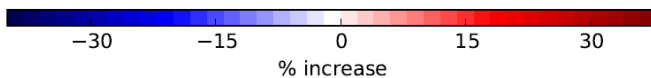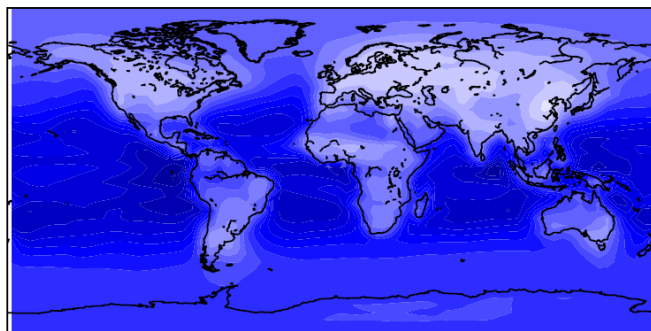
Figure 9. Percentage increase in **(a)** [PAN] and **(b)** [NO] of varying $k_{(R5)}$ from the IUPAC value ($k_{(R5)} = 1.4 \times 10^{-11}$ cm^3 molecule^{-1} s^{-1}) to that of the current study ($k_{(R5)} = 2.4 \times 10^{-11}$ cm^3 molecule^{-1} s^{-1}).

Title Page

Abstract | Introduction

Conclusions | References

Tables | Figures

|◀ | ▶|

◀ | ▶

Back | Close

Full Screen / Esc

Printer-friendly Version

Interactive Discussion